NICHOLAS SCHOOL OF THE ENVIRONMENT
DUKE UNIVERSITY

DIVISION OF EARTH & OCEAN SCIENCES

Thursday, September 28, 2017

Jack Middelburg
Editor
Biogeosciences

Dear Dr. Middelburg,

We would first like to thank you for your careful examination of our manuscript. We have taken into account your comments in the revised manuscript.

Below is a response to your comments and the revised manuscript. Please do not hesitate to contact us should you have any additional questions or comments on our manuscript.

Sincerely,
Zuchuan Li

Division of Earth and Ocean Sciences
Nicholas School of the Environment
Duke University
email. zuchuan.li@duke.edu

We thank the editor for his careful review of our manuscript. Below, we provide a response to the editor's comments.

line 32: meta-analysis (for readability).
Following the editor's comment, "meta analysis" has been replaced with "meta-analysis".

line 65, 344: replace on the other hand with however or alike because there is no on the one hand (and they always go together).
Following the editor's comment, "on the other hand" has been replaced with "however".

line 112: are assumed to be constant/uniform. The logic of calling half-saturation constants well mixed is not clear. Constant is also what matters.
Following the editor's comment, "well mixed" has been replaced with "constant/uniform".

A mechanistic model of an upper bound on oceanic carbon export as a function of mixed layer depth and temperature

Zuchuan Li*, Nicolas Cassar

Division of Earth and Ocean Sciences, Nicholas School of the Environment, Duke University, Durham, North Carolina, USA

* Corresponding author: Zuchuan Li (zuchuan.li@duke.edu)

Key points

1. A mechanistic model of an upper bound on carbon export is developed based on the metabolic balance of photosynthesis and respiration in the oceanic mixed layer
2. Using parameters available in the literature, the modeled upper bound envelopes field observations of export production estimated from ^{234}Th and sediment traps and O_2/Ar-derived net community production
3. The model identifies regions of the Southern Ocean where carbon export is likely limited by light during part of the growing season

Abstract

Export production reflects the amount of organic matter transferred from the surface ocean to depth through biological processes. This export is in great part controlled by nutrient and light availability, which are conditioned by mixed layer depth (MLD). In this study, building on Sverdrup's critical depth hypothesis, we derive a mechanistic model of an upper bound on carbon export based on the metabolic balance between photosynthesis and respiration as a function of MLD and temperature. We find that the upper bound is a positively skewed bell-shaped function of MLD. Specifically, the upper bound increases with deepening mixed layers down to a critical depth, beyond which a long tail of decreasing carbon export is associated with increasing heterotrophic activity and decreasing light availability. We also show that in cold regions the upper bound on carbon export decreases with increasing temperature when mixed layers are deep, but increases with temperature when mixed layers are shallow. A meta-analysis shows that our model envelopes field estimates of carbon export from the mixed layer. When compared to satellite export production estimates, our model indicates that export production in some regions of the Southern Ocean, most particularly the Subantarctic Zone, is likely limited by light for a significant portion of the growing season.

Key words: Export production, net community production, upper bound, mixed layer depth, temperature

1. Introduction

Photosynthesis in excess of respiration at the ocean surface leads to the production of organic matter, part of which is transported to the deep ocean through sinking and mixing (Volk and Hoffert, 1985). This biological process, known as export production (aka soft tissue biological carbon pump) lowers carbon dioxide (CO_2) concentrations at the ocean surface and facilitates the flux of CO_2 from the atmosphere into the ocean (Falkowski et al., 1998; Ito and Follows, 2005; Sigman and Boyle, 2000).

Export production is frequently assumed to be a function of net community production (NCP) which is defined as the balance between net primary production (NPP) and heterotrophic respiration (HR), or the difference between gross primary production (GPP) and community respiration (CR; HR plus autotrophic respiration (AR)) (the acronyms used in this study are presented in Table 1) (Li and Cassar, 2016):

$$CO_2 + H_2O \xrightarrow{\underbrace{\underbrace{GPP}_{NCP} \quad HR}_{NPP} \quad AR} Organic\ matter + O_2 \qquad (1)$$

$$Export\ production = NCP - MLD \times \frac{d(POC + DOC)}{dt} \qquad (2)$$

where POC, DOC and MLD represent particulate organic carbon, dissolved organic carbon and mixed layer depth, respectively. If the organic carbon inventory (POC+DOC) in the mixed layer is at steady state, NCP is equal to export production (equation (2)). Without allochthonous sources of organic matter, if the organic matter inventory in the mixed layer decreases, NCP will be predicted to be transiently smaller than export production. Conversely, export may lag NPP (Henson et al., 2015; Stange et al., 2017), in which case NCP is expected to be greater than export production.

Net community production is in great part regulated by the availability of nutrients and light. Light availability exponentially decays with depth due to absorption by water and its constituents. The mixing of phytoplankton to depth therefore impacts phytoplankton physiology and productivity (Cullen and Lewis, 1988; Lewis et al., 1984), with the depth-integrated NPP expected to increase down to the euphotic depth. Respiration, ~~on the other hand~~however, is often modeled to be some function of organic matter concentration, which is expected to be constant with depth if homogenously mixed within the mixed layer. Temperature is also believed to be an important control on carbon export because respiration is more temperature-sensitive than photosynthesis (Laws et al., 2000; López-Urrutia et al., 2006; Rivkin and Legendre, 2001). Field observations confirm that NCP is generally lower at high temperatures and consistently low when mixed layers are deep. These patterns have been attributed to the balance between depth-integrated photosynthesis (controlled by the availability of nutrients and light) and respiration as a function of MLD and temperature (Cassar et al., 2011; Eveleth et al., 2016; Huang et al., 2012; Shadwick et al., 2015; Tortell et al., 2015). However, descriptions of the underlying mechanisms heretofore remain qualitative. Likewise, the effects of light and nutrient on carbon fluxes are difficult to disentangle. For example, high-nutrient, low-chlorophyll regimes in the Southern Ocean have been attributed to iron limitation (Boyd et al., 2000), deep mixed layers and light limitation (Nelson and Smith, 1991; Mitchell and Holm-Hanse, 1991; Mitchell et al., 1991), or both (Sunda and Huntsman, 1997). To decompose the influence of light and nutrient availability on NCP, we define the upper bound on carbon export from the mixed layer (NCP^*) as the maximum export achievable should all limiting factors other than light (taking into account self-shading) be alleviated.

In his seminal paper, Sverdrup presented an elegant model to demonstrate that vernal phytoplankton blooms (i.e., organic matter accumulation at the ocean surface) may be driven by

84 increased light availability when the MLD shoals above a critical depth (Z_c) (Sverdrup, 1953). In
85 our study, we build upon Sverdrup (1953) and derive a mechanistic model of an upper bound on
86 carbon export based on the metabolic balance of photosynthesis and respiration in the oceanic
87 mixed layer, where the metabolic balance is derived from MLD, temperature, photosynthetically
88 active radiation (PAR), phytoplankton maximum growth rate (μ_{max}), and heterotrophic activity.
89 Our approach is analogous to other efforts where mechanistic models were derived to predict
90 proxies of carbon export (e.g., Dunne et al. (2005) and Cael and Follows (2016)). We compare our
91 NCP^* model to observations, and use this model in conjunction with satellite export production
92 estimates to identify regions in the world's oceans where light may limit export production. Our
93 key findings are that 1) using parameters available in the literature, the modeled upper bound
94 envelopes field observations of export production estimated from ^{234}Th and sediment traps and
95 O_2/Ar-derived NCP, and 2) the model identifies regions of the Southern Ocean where carbon
96 export is likely limited by light during part of the growing season.

97 **2. Model description and comparison to observations**

98 **2.1. Net community production and light availability**

99 A conceptual representation of the metabolic balance between volumetric NCP, NPP, and HR
100 profiles is presented in Figure 1(A). According to equation (1), the volumetric NCP flux at a given
101 depth (z) in the mixed layer results from the difference between volumetric NPP and HR:

102 $$NCP(z) = NPP(z) - HR(z) \qquad (3)$$

103 where z increases with depth. $NPP(z)$ is a function of the autotroph's intrinsic growth rate
104 (μ) times their biomass concentration (C). Assuming that the effect of nutrients and light on
105 photosynthetic rates abides by Michaelis-Menten kinetics, and neglecting the effect of

photoinhibition (Dutkiewicz et al., 2001; Huisman and Weissing, 1994), $NPP(z)$ may be expressed as follows:

$$NPP(z) = \mu(z) \times C = \frac{N}{N + k_m^N} \times \frac{I(z)}{I(z) + k_m^I} \times \mu_{max} \times C \qquad (4)$$

where μ_{max} is the maximum intrinsic growth rate of the autotrophic community; N and k_m^N represent the nutrient concentration and half-saturation constant, respectively; and I and k_m^I represent the irradiance level and half-saturation constant, respectively. μ_{max}, N, k_m^N, k_m^I and C are assumed to be ~~well mixed~~constant/uniform within the mixed layer. The first two terms on the right-hand side of equation (4) account for the effect of nutrient and light availability on autotrophic growth rates, and they are hereafter defined as follows for simplicity:

$$N_m = \frac{N}{N + k_m^N} \qquad (5a)$$

$$I_m(z) = \frac{I(z)}{I(z) + k_m^I} \qquad (5b)$$

$I(z)$ is modeled as an exponential decay of PAR just beneath the water surface (I_0):

$$I(z) = I_0 \times e^{-K_I \times z} \qquad (6)$$

where K_I is light attenuation coefficient which is assumed to be independent of depth in the mixed layer.

As a first approximation, we assume that $HR(z)$ is proportional to C as in previous studies (Dutkiewicz et al., 2001; Huisman and Weissing, 1994; Rivkin and Legendre, 2001; Sverdrup, 1953; White et al., 1991):

$$HR(z) = r_{HR} \times C \qquad (7)$$

where r_{HR} represents the intrinsic heterotrophic respiration rate which is assumed to be dependent on temperature (see below), and independent of depth. In reality, $HR(z)$ is likely best modeled as

a function of the concentration of labile organic matter — an additional term could be included to account for the relationship of total labile organic matter to C.

NCP integrated over the mixed layer ($NCP(0, MLD)$) can be derived from equations (3-7):

$$NCP(0, MLD) = NPP(0, MLD) - HR(0, MLD)$$

$$= \int_0^{MLD} NPP(z)dz - \int_0^{MLD} HR(z)dz$$

$$= N_m \times I_m(0, MLD) \times \mu_{max} \times C - r_{HR} \times MLD \times C \quad (8)$$

The first term on the right side of equation (8) represents NPP integrated over the mixed layer ($NPP(0, MLD)$), which is equivalent to the product of $\int_0^{MLD} \mu(z)dz$ and C, where the former term is modeled to be a function of μ_{max} conditioned by nutrient and light availability within the mixed layer. $I_m(0, MLD)$ can be derived as follows:

$$I_m(0, MLD) = \int_0^{MLD} I_m(z)dz = -\frac{1}{K_I} \times ln\left(\frac{I_0 \times e^{-K_I \times MLD} + k_m^I}{I_0 + k_m^I}\right) \quad (9)$$

NCP integrated over the mixed layer (equation (8)) is a bell-shaped function of MLD as depicted in the schematic diagram of Figure 1(B).

2.2. Net community production and phytoplankton biomass concentration

As can be seen from equation (8), $NCP(0, MLD)$ is a direct function of C because $NPP(0, MLD)$ and $HR(0, MLD)$ are proportional to C. $NCP(0, MLD)$ is also an indirect function of C due its effect on light attenuation (i.e., K_I). The attenuation coefficient K_I can be divided into water and non-water components ($K_I = K_I^w + K_I^{nw}$) (Baker and Smith, 1982; Smith and Baker, 1978a; Smith and Baker, 1978b), where K_I^{nw} is controlled by the concentrations of phytoplankton, colored dissolved organic matter (CDOM), and non-algal particles (NAP). In the open ocean where CDOM and NAP co-vary with phytoplankton (Morel and Prieur, 1977), K_I can be related to C as follows:

$$K_I = K_I^w + k_c \times C \quad (10)$$

where k_c is a function of the solar zenith angle, the specific absorption and backscattering coefficients of phytoplankton, and the relationship between phytoplankton, CDOM, and NAP. Because pure water and phytoplankton attenuate light, K_I^w and k_c should be greater than zero.

To calculate how $NCP(0, MLD)$ varies as a function of C, we examine its first ($\frac{dNCP(0,MLD)}{dC}$) and second ($\frac{d^2NCP(0,MLD)}{dC^2}$) derivatives with respect to C based on equations (8) and (10):

$$\frac{dNCP(0,MLD)}{dC}$$

$$= N_m \times \mu_{max} \times \frac{K_I^w \times I_m(0,MLD) + k_c \times C \times MLD \times I_m(MLD)}{K_I^w + k_c \times C} - r_{HR} \times MLD \quad (11)$$

$$\frac{d^2NCP(0,MLD)}{dC^2} = N_m \times k_c \times \frac{\mu_{max}}{K_I}$$

$$\times \left\{ \frac{2 \times K_I^w}{K_I} \times \left(MLD \times I_m(MLD) - I_m(0,MLD) \right) - \frac{k_c \times C \times I_m(MLD)^2 \times MLD^2 \times k_m^I}{I_0 \times e^{-K_I \times MLD}} \right\} \quad (12)$$

when $MLD > 0$, $I_m(0,MLD) > MLD \times I_m(MLD)$:

$$I_m(0,MLD) = \int_0^{MLD} \frac{I_0 \times e^{-K_I \times z}}{I_0 \times e^{-K_I \times z} + k_m^I} dz$$

$$> \int_0^{MLD} \frac{I_0 \times e^{-K_I \times MLD}}{I_0 \times e^{-K_I \times MLD} + k_m^I} dz = MLD \times I_m(MLD) \quad (13)$$

The detailed derivation of equations (11-12) can be found in the supplementary material. Substituting the inequality (13) into equation (12) gives $\frac{d^2NCP(0,MLD)}{dC^2} < 0$, which suggests that $\frac{dNCP(0,MLD)}{dC}$ decreases with increasing C. Because increasing C decreases light availability due to shelf-shading, $NPP(0,MLD)$ saturates with increasing C. Thus, $NCP(0,MLD)$ will reach an asymptote of $\lim_{C \to \infty} \left(\frac{dNCP(0,MLD)}{dC} \right) = -r_{HR} \times MLD < 0$, because $HR(0,MLD)$ linearly increases

with increasing C while $NPP(0, MLD)$ plateaus (Figure 2). Additionally, because $NCP(0, MLD)$ must be nil when there is no autotrophic biomass ($NCP(0, MLD)|_{C=0} = 0$), $\lim_{C \to 0}\left(\frac{dNCP(0,MLD)}{dC}\right)$ must be greater than zero, otherwise the ecosystem would be net heterotrophic which is unachievable without an allochthonous source of organic matter. $\lim_{C \to 0}\left(\frac{dNCP(0,MLD)}{dC}\right) > 0$ and $\lim_{C \to \infty}\left(\frac{dNCP(0,MLD)}{dC}\right) = -r_{HR} \times MLD < 0$ suggest the existence of $\frac{dNCP(0,MLD)}{dC}\Big|_{C=C^*} = 0$ where C^* corresponds to an autotrophic biomass concentration which maximizes $NCP(0, MLD)$ (i.e., NCP^*).

The dependence of $NCP(0, MLD)$ on C can be conceptually understood in the following way. Given a water column with sufficient nutrients, the critical depth Z_c and compensation depth Z_p are expected to shoal as C increases. When C is low, $NCP(0, MLD)$ increases with C because of its greater impact on $NPP(0, MLD)$ than on $HR(0, MLD)$. As C further increases, the increase in $NPP(0, MLD)$ with C slows because of light attenuation (i.e., K_I). There is therefore a C^* which maximizes the difference between $NPP(0, MLD)$ and $HR(0, MLD)$ leading to NCP^* (Figure 2). Beyond this point (C^*), further increasing C will cause self-shading and limit photosynthesis in the deep part of the mixed layer, as a result decreasing $NCP(0, MLD)$. Beyond a critical biomass (C_c), the ecosystem becomes net heterotrophic. Without an allochthonous source of organic carbon, this is only transiently sustainable.

2.3. Mixed layer depth and compensation depth

By definition, if $NCP(MLD)$ is ~~smaller~~ less than zero (i.e., net heterotrophy at the bottom of the mixed layer), the MLD must be deeper than Z_p ($MLD > Z_p$) (and vice versa). To determine the sign of $NCP(MLD)$, we substitute inequality (13) into equation (11). According to the inequality presented in equation (13), $\frac{K_I^W \times I_m(0,MLD) + k_c \times C \times MLD \times I_m(MLD)}{K_I^W + k_c \times C}$ in equation (11) must be

greater than $\frac{K_I^W \times MLD \times I_m(MLD) + k_c \times C \times MLD \times I_m(MLD)}{K_I^W + k_c \times C}$ (which is equal to $MLD \times I_m(MLD)$). After simple rearrangements, the substitution of inequality (13) into equation (11) leads to:

$$\frac{dNCP(0, MLD)}{dC}$$

$$> MLD \times (N_m \times I_m(MLD) \times \mu_{max} - r_{HR}) = \frac{MLD}{C} \times NCP(MLD) \qquad (14)$$

The inequality in equation (14) in turn suggests that when $NCP(0, MLD)$ is maximized ($\frac{dNCP(0,MLD)}{dC} = 0$), $NCP(MLD)$ is negative (net heterotrophic) and hence the MLD is deeper than Z_p ($MLD > Z_p$). This counterintuitive result is attributable both to the uneven distribution of light availability in the water column (equation (13)) and to water which absorbs light but does not contribute to biomass accumulation. When the mixed layer is at the Z_p, a slight increase in C will leads to negative $NCP(MLD)$ due to decreasing light availability at the base of mixed layer, but will increase NCP higher in the water column because of the increase in biomass. The increase in NCP in the shallow parts of the mixed layer therefore overcompensates for the net heterotrophy at the bottom of the mixed layer, thus maximizing the depth-integrated NCP. If light were uniformly distributed in the water column (i.e., $I_m(0, MLD) = MLD \times I_m(MLD)$) and if water did not attenuate light ($K_I^W = 0$ in equation (11)), $MLD = Z_p$ would maximize $NCP(0, MLD)$, which is consistent with Huisman and Weissing (1994). We note that in equation (14) the NCP profile ($NCP(z)$) varies with increasing C, which is different from what is conceptually presented in Figure 1. The depth-integrated NCP in Figure 1 maximizes at the compensation depth because the NCP profile ($NCP(z)$) is assumed to be invariant.

2.4. An upper bound on carbon export

Equations (11-13) delineate the conditions for an upper bound on carbon export (NCP^*). In order to simplify the relationship of NCP^* to MLD and temperature, we approximate $I_m(0, MLD)$:

$$I_m(0, MLD) = -\frac{1}{K_I} \times ln\left(1 + \frac{I_0}{I_0 + k_m^I} \times (e^{-K_I \times MLD} - 1)\right)$$

$$\approx -\frac{1}{K_I} \times ln\big(1 - I_m(0)\big) \qquad (15)$$

where $I_m(0) = \frac{I_0}{I_0 + k_m^I}$. Based on equation (15), $NCP(0, MLD)$ in equation (8) can be approximated as:

$$NCP(0, MLD) = C \times MLD \times \left(\frac{1}{K_I \times MLD} \times \mu^* - r_{HR}\right) \qquad (16)$$

where $\mu^* = -ln\big(1 - I_m(0)\big) \times N_m \times \mu_{max}$. To evaluate the approximation accuracy of equation (15), we compare the upper bounds estimated from equation (16) and the original model (equations (8-10)). Our comparison suggests that the approximation of equation (15) is accurate for the estimation of NCP^* under most conditions (Figure 3).

We first need to derive the C^* which maximizes $NCP(0, MLD)$ (i.e., NCP^*) in equation (16). C^* can be solved from the first derivative of $NCP(0, MLD)$ in equation (16) with respect to C:

$$\left.\frac{dNCP(0, MLD)}{dC}\right|_{NCP(0,MLD)=NCP^*} = \mu^* \times \frac{K_I^W}{(k_c \times C^* + K_I^W)^2} - MLD \times r_{HR} = 0 \qquad (17)$$

and therefore:

$$C^* = \frac{1}{k_c} \times \left[-K_I^W + \sqrt{\frac{\mu^* \times K_I^W}{MLD \times r_{HR}}}\right] \qquad (18)$$

Equation (18) decreases with MLD. As C^* is positive ($C^* \geq 0$) and cannot go to infinity ($C^* \leq C_{max}^*$), MLD should satisfy $MLD_{C_{max}^*} \leq MLD \leq \frac{\mu^*}{r_{HR} \times K_I^W}$, where $MLD_{C_{max}^*}$ represents the MLD corresponding to the maximum achievable autotroph's biomass concentration (C_{max}^*) in the surface ocean. The NCP^* model for $0 \leq MLD < MLD_{C_{max}^*}$ is not discussed here, because we do

not have data with very shallow MLD to constrain and evaluate the model. The derivation of the model is however presented in the supplementary material. Substituting C^* from equation (18) into equation (16):

$$\sqrt{NCP^*} = a_2 \times \sqrt{-ln\left(1 - I_m(0)\right)} + a_1 \times \sqrt{MLD} \qquad (19)$$

where $a_1 = -\sqrt{\frac{K_I^W \times r_{HR}}{k_c}}$ and $a_2 = \sqrt{\frac{N_m \times \mu_{max}}{k_c}}$. Constants a_1 and a_2 are functions of r_{HR} and μ_{max}, respectively, which are generally modeled to increase with temperature (T) (Eppley, 1972; Rivkin and Legendre, 2001):

$$\mu_{max} = \mu_{max}^0 \times e^{P_t \times T} \qquad (20a)$$

$$r_{HR} = r_{HR}^0 \times e^{B_t \times T} \qquad (20b)$$

where P_t and B_t are constants; and μ_{max}^0 and r_{HR}^0 are maximum growth rate and heterotrophic respiration ratio for $T = 0$ °C, respectively. P_t is commonly assumed to equal 0.0663 (Eppley, 1972). Substituting equations (20a) and (20b) into equation (19) yields:

$$\sqrt{NCP^*} = a_4 \times \sqrt{e^{P_t \times T}} \times \sqrt{-ln\left(1 - I_m(0)\right)} + a_3 \times \sqrt{e^{B_t \times T}} \times \sqrt{MLD} \qquad (21)$$

where $a_3 = -\sqrt{\frac{r_{HR}^0 \times K_I^W}{k_c}}$ and $a_4 = \sqrt{\frac{\mu_{max}^0 \times N_m}{k_c}}$.

2.5. Comparison to observations

2.5.1 Data products

We assess the performance of our modeled upper bound on carbon export using a global dataset of MLD, PAR, sea surface temperature (SST), O_2/Ar-derived NCP, and export production derived from sediment traps and ^{234}Th (see supplementary material). MLD was derived from global Argo profiles (Global Ocean Data Assimilation Experiment; http://www.usgodae.org/) and CTD casts (National Oceanographic Data Center; https://www.nodc.noaa.gov/). PAR was downloaded from

the NASA ocean color website (https://oceancolor.gsfc.nasa.gov/). The NCP estimates are based on a compilation of O_2/Ar measurements from Li and Cassar (2016), Li et al. (2016), Shadwick et al. (2015), and Martin et al. (2013). The POC export production estimates were obtained from the recently compiled dataset of Mouw et al. (2016). These estimates were adjusted to reflect a flux at the base of mixed layer using the Martin curve of organic carbon attenuation with depth (Martin et al., 1987). The constants k_c and K_I^w in equation (10) were derived assuming a carbon to chlorophyll *a* ratio of 90 (Arrigo et al., 2008) and an empirical linear relationship between K_I and chlorophyll *a* concentration (see Figure S3), calculated based on the NOMAD dataset (Werdell and Bailey, 2005). k_m^I was set at 4.1 Einstein m^{-2} d^{-1} following Behrenfeld and Falkowski (1997). In our estimation of the upper bound on carbon export, we set N_m to 1 in the NCP^*calculations.

2.5.2 Results and discussion

Overall, we find that NCP^* calculated using published parameters (Table 2) does a good job of enveloping carbon export observations reported in the literature (Figure 4(A)). Samples on the NCP^* envelope (upper bound) are likely regulated by light availability. Conversely, points below the upper bound may be nutrient limited. As expected, NCP^* increases with μ_{max} and decreases with r_{HR}. Model parameters $a_1 = -1.78$and $a_2 = 14.75$ (equation (19)) provide the best fit to the upper bound of O_2/Ar-NCP as a function of MLD. When compared to parameters available in the literature (Table 2), we find that the best fit to our modeled upper bound is using μ_{max} and r_{HR} of 1.2 d^{-1} and 0.2 d^{-1}, respectively. When accounting for the effect of T on μ_{max} and r_{HR}, model constants $a_3 = -1.53$ and $a_4 = 13.39$ (equation (21)) best fit the upper bound on O_2/Ar-NCP, SST and MLD observations.

Our results show that NCP^* decreases faster with increasing MLD in warmer waters (Figures 4(B) and 4(C)), because the term $a_3 \times \sqrt{e^{B_t \times T}}$ in equation (21) is negative and negatively

correlated to T. This temperature effect contributes to part of the relationship between export production and MLD in Figure 4(A). Interestingly, NCP^* increases with T in colder waters and shallow mixed layers (Figure 4(C)). This is because NCP^* reflects the balance between productivity ($a_4 \times \sqrt{e^{P_t \times T}} \times \sqrt{-ln\left(1 - I_m(0)\right)}$) and heterotrophic respiration ($a_3 \times \sqrt{e^{B_t \times T}} \times \sqrt{MLD}$). In a shallow cold mixed layer, the change in productivity with T ($\frac{d\left(a_4 \times \sqrt{e^{P_t \times T}} \times \sqrt{-ln\left(1-I_m(0)\right)}\right)}{dT} = \frac{P_t}{2} \times a_4 \times \sqrt{e^{P_t \times T}} \times \sqrt{-ln\left(1 - I_m(0)\right)}$) is greater than that of heterotrophic respiration ($\frac{d\left(a_3 \times \sqrt{e^{B_t \times T}} \times \sqrt{MLD}\right)}{dT} = \frac{B_t}{2} \times a_3 \times \sqrt{e^{B_t \times T}} \times \sqrt{MLD}$). These results could explain part of the variability in the relationship between NCP and SST reported in previous studies (Li and Cassar, 2016). Our NCP^* model does not perform as well in warmer deep mixed layers, where high variability in export ratio maxima have also been reported (Cael and Follows, 2016). This may stem from uncertainties in observations, the differing relationship between T, μ_{max}, and r_{HR} at high temperature, and/or violations of our assumptions (see caveats and limitations).

Several recent studies have explored the relationship of NCP to oceanic parameters based on various statistical approaches (Cassar et al., 2015; Chang et al., 2014; Huang et al., 2012; Li and Cassar, 2016; Li et al., 2016). Our model can shed some light into the mechanisms driving some of these patterns. To that end, we substitute equation (9) into equation (8):

$$NCP(0, MLD) = C \times MLD \times \left(-\frac{N_m \times \mu_{max}}{K_I \times MLD} \times ln\left(\frac{I_0 \times e^{-K_I \times MLD} + k_m^I}{I_0 + k_m^I} \right) - r_{HR} \right) \quad (22)$$

Rearranging equation (22):

$$NCP_B = \frac{NCP(0, MLD)}{C \times MLD} = -\frac{ln\left(\frac{I_0 \times e^{-K_I \times MLD} + k_m^I}{I_0 + k_m^I} \right)}{I_0 \times (1 - e^{-K_I \times MLD})} \times N_m \times \mu_{max} \times PAR_{ML} - r_{HR} \quad (23)$$

where NCP_B is the biomass-normalized volumetric NCP, PAR_{ML} is the average PAR in the mixed layer ($PAR_{ML} = \frac{1-e^{-K_I \times MLD}}{K_I \times MLD} \times I_0$), and $-\frac{ln\left(\frac{I_0 \times e^{-K_I \times MLD} + k_m^I}{I_0 + k_m^I}\right)}{I_0 \times \left(1-e^{-K_I \times MLD}\right)} \times N_m \times \mu_{max}$ and $-r_{HR}$ correspond to the slope and offset, respectively. The scatter in the relationship between chlorophyll-normalized volumetric NCP and PAR_{ML}, as reported in previous studies (Bender et al., 2016), can likely be explained by the effect of temperature and the availability of nutrient and light (among other properties) on the slope and offset of equation (23). Equation (22) can also be reorganized to assess how environmental conditions may impact the export ratio (ef):

$$ef = \frac{NCP(0, MLD)}{NPP(0, MLD)} = 1 - \frac{K_I \times MLD}{-ln\left(\frac{I_0 \times e^{-K_I \times MLD} + k_m^I}{I_0 + k_m^I}\right)} \times \frac{1}{N_m} \times \frac{r_{HR}}{\mu_{max}} \qquad (24)$$

where $\frac{r_{HR}}{\mu_{max}}$ is proportional to $e^{(B_t - P_t) \times T}$. Equation (24) is consistent with multiple studies which predict decreasing ef with increasing temperature (Cael and Follows, 2016; Dunne et al., 2005; Henson et al., 2011; Laws et al., 2000; Li and Cassar, 2016). In fact, equation (5) of Cael and Follows (2016) can easily be derived from equation (24) (see supplementary material). Equation (24) also highlights that a multitude of factors may confound the dependence of ef on temperature (including varying MLD, light attenuation, and availability of nutrient and light). This again may explain some of the conflicting observations recently reported in the literature (e.g., Maiti et al. (2013)), where the effect of temperature may be masked by changes in community composition (Britten et al., 2017; Henson et al., 2015). One therefore needs to account or correct for the multitude of confounding factors when predicting the effect of a given environmental condition (e.g., temperature, mineral ballast, and NPP) on the export ratio.

3. Spatial distribution of the upper bound on carbon export

We estimate the global distribution of the upper bound of carbon export using equation (19) and climatological monthly MLD and PAR. In general, NCP^* is high in low latitudes and low in the North Atlantic and Antarctic Circumpolar Current (ACC) in the Southern Ocean (Figure 5(A)). As expected, this spatial pattern is controlled by MLD (see Figure S1). Satellite-derived estimates of NCP (Li and Cassar, 2016) are approximately 10% of global NCP^* , reflecting the high degree of nutrient limitation in the oceans. We also derive a global NCP^* map using equation (21), and find that the global NCP^* estimate is very sensitive to the temperature dependence of r_{HR}. For example, decreasing the B_t in $r_{HR} = r_{HR}^0 \times e^{B_t \times T}$ from 0.11 to 0.08 (as used in Rivkin and Legendre (2001) and López-Urrutia et al. (2006)) increases the global NCP^* budget by a factor of 2.4. Large differences in NCP^* in low-latitudes in great part explain this change. In light of the large uncertainties in the relationship between r_{HR} and T (Cael and Follows, 2016; López-Urrutia et al., 2006), we hereafter only discuss NCP^* estimates derived from equation (19).

To estimate how close export production is to its upper bound, we calculate the ratio of export production to NCP^* (f_{pt}). Low f_{pt} regimes represent ecosystems likely regulated by nutrient availability (i.e., ecosystems that have not reached their full export potential based on MLD and surface PAR). As expected, low latitude and subtropical regions have low f_{pt} (Figure 5(B)). High f_{pt} regimes represent ecosystems which have reached their full light potential, and are therefore less likely to respond to nutrient addition because of light limitation (e.g., North Atlantic and ACC (Figure 5(B))). In these regions, especially the subantarctic region, f_{pt} is high in the spring (Figure 5(C)) and decreases in the summer (Figure 5(D)), suggesting that export production is likely co-limited by nutrient and light availability. This may in part explain the lower response to iron fertilization in the subantarctic region where substantial increases in surface chlorophyll were only

observed in regions with shallower mixed layers (Boyd et al., 2007; Boyd et al., 2000; de Baar et al., 2005).

Also shown in Figure 5 are the biological pump efficiency and export ratio ef (panels 5E and 5F, respectively). These various proxies reflect different components of the biological pump. Whereas f_{pt} reflects the export potential based on current MLD and light availability, the biological pump efficiency reflects the potential as derived from nutrient distribution in the oceans, estimated from the extent of nutrient removal from the surface ocean (Sarmiento and Gruber, 2006) or the proportion of regenerated nutrients at depth (Ito and Follows, 2005). A revised estimate of the global biological pump efficiency, estimated based on the proportion of regenerated to total nutrients (preformed + regenerated) at depth is around 30-35% (Duteil et al., 2013). The ef ratio ~~on the other hand~~however describes how much of production is exported as opposed to recycled in the surface (Dunne et al., 2005). The ultra-oligotrophic subtropical waters have a low export ratio, a strong biological pump efficiency with exhaustion of nutrients at the ocean surface, and therefore have not reached their full light potential (low f_{pt}) because of the strong stratification and nutrient limitation. The seasonal pattern of f_{pt} in the subantarctic region suggests that the low biological pump efficiency is the result of light limitation in the austral spring and nutrient (likely Fe) and light limitation in the austral summer.

4. Caveats and limitations

There are a multitude of uncertainties, simplifications, and approximations in our model and field observations. Among others:

- In our study, we used a model which builds on Sverdrup's critical depth hypothesis. There are competing hypotheses to explain phytoplankton bloom phenology (timing and intensity), including the "dilution recoupling hypothesis" or "disturbance recovery

hypothesis" (Behrenfeld, 2010; Boss and Behrenfeld, 2010) and "critical turbulence hypothesis" (Brody and Lozier, 2015; Huisman et al., 1999; Taylor and Ferrari, 2011). In the case of top-down control, any respiratory grazing loss not accounted for by our loss term would behave as a system not reaching its full light potential (NCP^* ~~NCP*~~). Conversely, any grazing loss associated with export (e.g., rapidly sinking fecal pellets and other zooplankton-mediated export pathways) would minimize respiratory losses thereby bringing NCP closer to its upper bound based on light-availability. These opposing effects are beyond the scope of this study, but could be modeled, especially as we learn more about their impacts on carbon fluxes through new efforts such as NASA's EXPORTS program (Siegel et al., 2016). See also the point below on mixing vs. mixed layer depth.

- Phytoplankton biomass concentration (C) may vary with depth in the mixed layer, especially for water columns experiencing varying degrees of turbulent mixing. In addition, MLD is not always the best proxy of light availability with mixing layer in some cases deviating from the mixed layer (Franks, 2015; Huisman et al., 1999). The factors defining the MLD also vary in different oceanic regions.
- For simplicity, we model the dependence of photosynthesis on irradiance assuming Michaelis-Menten kinetics, which does not account for photoinhibition. More accurate models can be found in other studies (Platt et al., 1980). Due to optional absorption, K_I also varies with depth in the mixed layer. Additionally, the linear relationship between K_I and C is influenced by CDOM, NAP, and other environmental factors (e.g., solar zenith angle) (Gordon, 1989).
- μ_{max} and r_{HR} are influenced by environmental factors other than temperature, including community structure (Chen and Laws, 2017), and may vary with depth within the mixed

layer (Smetacek and Passow, 1990). For these reasons, the equations relating μ_{max} and r_{HR} (i.e., B_t and P_t) to temperature also carry significant uncertainties (Bissinger et al., 2008; Edwards et al., 2016; Kremer et al., 2017; López-Urrutia and Morán, 2007; Rivkin and Legendre, 2001) which impacts our estimates of the upper bound on carbon export, especially in warmer regions. As in other recent studies (Cael and Follows, 2016; Cael et al., 2017; Dutkiewicz et al., 2001; Gong et al., 2015; Gong et al., 2017; Huisman et al., 2006; Taylor and Ferrari, 2011), we model heterotrophic respiration to vary in proportion to phytoplankton concentration. The model could be further improved by explicitly including the concentration of heterotrophs. See point above on the grazing effect on export with regards to r_{HR}.

- NCP may underestimate export production when accompanied by a decrease in the inventory of organic matter in the mixed layer (see introduction and equation (2)).
- Our field observations are limited, mostly focusing on the spring and summer seasons, and harbor significant uncertainties. For example, deep mixed layers can bias the O_2/Ar method low if entrainment of deeper waters brings low O_2 into the mixed layer. Descriptions of these uncertainties are presented in other studies (Bender et al., 2011; Cassar et al., 2014; Jonsson et al., 2013).
- Finally, our study is only relevant to the mixed layer. It does not account for productivity below the mixed layer, which can be important in some regions such as the subtropical ocean.

5. Conclusions

In this study, we derived a mechanistic model of an upper bound on carbon export (NCP^*) based on the metabolic balance between photosynthesis and respiration of the plankton community. The

upper bound is a positively skewed bell-shaped function of mixed layer depth (MLD). At low temperatures, the upper bound decreases with temperature if mixed layers are deep, but increases with temperature if mixed layers are shallow. We used this model to derive a global distribution of an upper bound on carbon export as a function of MLD and surface PAR, which shows high values in low latitudes and low values in high latitudes due to deep MLD. To examine how current export production compares to this upper bound in the world's oceans, we calculated the ratio of satellite export production estimates to the upper bound derived by our model. High ratios of export production to NCP^* in the North Atlantic and ACC indicate that export production in these regions is likely co-limited by nutrient and light availability. Overall, our results may explain differences in carbon export measured during past iron fertilization experiments (e.g., subantarctic and polar regions), inform future iron fertilization experiments, help in the development of remotely-sensed carbon export algorithms, and improve predictions of the response of marine ecosystems to a changing climate.

Acknowledgements

We would like to acknowledge NASA GSFC for processing and distributing PAR and SST products (http://oceancolor.gsfc.nasa.gov/). Global Argo temperature-salinity profiling floats were downloaded from http://www.usgodae.org/. CTD casts were downloaded from National Oceanographic Data Center (https://www.nodc.noaa.gov/). N.C. was supported by NSF OPP-1043339. Z.L. was supported by a NASA Earth and Space Science Fellowship (Grant No. NNX13AN85H). The authors thank three anonymous reviewers for their insightful comments.

References

Arrigo, K. R., van Dijken, G. L., and Bushinsky, S.: Primary production in the Southern Ocean, 1997-2006, J. Geophys. Res., 113, doi:10.1029/2007JC004551, 2008.

426 Baker, K. S. and Smith, R. C.: Bio-optical classification and model of natural waters .2, Limnol.
427 and Oceanogr., 27, 500-509, doi:10.4319/lo.1982.27.3.0500, 1982.
428 Behrenfeld, M. J.: Abandoning Sverdrup's Critical Depth Hypothesis on phytoplankton blooms,
429 Ecology, 91, 977–989, doi:10.1890/09-1207.1, 2010.
430 Behrenfeld, M. J. and Falkowski, P. G.: Photosynthetic rates derived from satellite-based
431 chlorophyll concentration, Limnol. and Oceanogr., 42, 1-20,
432 doi:10.4319/lo.1997.42.1.0001, 1997.
433 Bender, M. L., Tilbrook, B., Cassar, N., Jonsson, B. F., Poisson, A., and Trull, T. W.: Ocean
434 productivity south of Australia during spring and summer, Deep-Sea Res. Pt. I, 112, 68-78,
435 doi:10.1016/j.dsr.2016.02.018, 2016.
436 Bender, M. L., Kinter, S., Cassar, N., and Wanninkhof, R.: Evaluating gas transfer velocity
437 parameterizations using upper ocean radon distributions, J. Geophys. Res., 116,
438 doi:10.1029/2009JC005805, 2011.
439 Bissinger, J. E., Montagnes, D. J. S., Sharples, J., and Atkinson, D.: Predicting marine
440 phytoplankton maximum growth rates from temperature: Improving on the Eppley curve
441 using quantile regression, Limnol. Oceanogr., 53, 487–493,
442 doi:10.4319/lo.2008.53.2.0487, 2008.
443 Boss, E. and Behrenfeld, M. J.: In situ evaluation of the initiation of the North Atlantic
444 phytoplankton bloom, Geophys. Res. Lett., 37, doi:10.1029/2010GL044174, 2010.
445 Boyd, P. W., Jickells, T., Law, C. S., Blain, S., Boyle, E. A., Buesseler, K. O., Coale, K. H., Cullen,
446 J. J., de Baar, H. J. W., Follows, M., Harvey, M., Lancelot, C., Levasseur, M., Owens, N.
447 P. J., Pollard, R., Rivkin, R. B., Sarmiento, J., Schoemann, V., Smetacek, V., Takeda, S.,
448 Tsuda, A., Turner, S., and Watson, A. J.: Mesoscale iron enrichment experiments 1993-
449 2005: Synthesis and future directions, Science, 315, 612-617,
450 doi:10.1126/science.1131669, 2007.
451 Boyd, P. W., Watson, A. J., Law, C. S., Abraham, E. R., Trull, T., Murdoch, R., Bakker, D. C. E.,
452 Bowie, A. R., Buesseler, K. O., Chang, H., Charette, M., Croot, P., Downing, K., Frew, R.,
453 Gall, M., Hadfield, M., Hall, J., Harvey, M., Jameson, G., LaRoche, J., Liddicoat, M., Ling,
454 R., Maldonado, M. T., McKay, R. M., Nodder, S., Pickmere, S., Pridmore, R., Rintoul, S.,
455 Safi, K., Sutton, P., Strzepek, R., Tanneberger, K., Turner, S., Waite, A., and Zeldis, J.: A

456 mesoscale phytoplankton bloom in the polar Southern Ocean stimulated by iron
457 fertilization, Nature, 407, 695-702, doi:10.1038/35037500, 2000.
458 Britten, G. L., Wakamatsu, L., and Primeau, F. W.: The temperature-ballast hypothesis explains
459 carbon export efficiency observations in the Southern Ocean, Geophys. Res. Lett., 44,
460 1831-1838, doi:10.1002/2016GL072378, 2017.
461 Brody, S. R. and Lozier, M. S.: Characterizing upper-ocean mixing and its effect on the spring
462 phytoplankton bloom with in situ data, ICES J. Mar. Sci., 72, 1961–1970.
463 doi:10.1093/icesjms/fsv006, 2015
464 Cael B. B., Bisson, K., and Follows, M. J.: How have recent temperature changes affected the
465 efficiency of ocean biological carbon export? Limnology and Oceanography Letters, 2,
466 113-118, doi:10.1002/lol2.10042, 2017.
467 Cael, B. B. and Follows, M. J.: On the temperature dependence of oceanic export efficiency,
468 Geophys. Res. Lett., 43, 5170-5175, doi:10.1002/2016GL068877, 2016.
469 Cassar, N., Nevison, C. D., and Manizza, M.: Correcting oceanic O_2/Ar-net community production
470 estimates for vertical mixing using N_2O observations, Geophys. Res. Lett., 41, 8961-8970,
471 doi:10.1002/2014GL062040, 2014.
472 Cassar, N., DiFiore, P. J., Barnett, B. A., Bender, M. L., Bowie, A. R., Tilbrook, B., Petrou, K.,
473 Westwood, K. J., Wright, S. W., and Lefevre, D.: The influence of iron and light on net
474 community production in the Subantarctic and Polar Frontal Zones, Biogeosciences, 8,
475 227-237, doi:10.5194/bg-8-227-2011, 2011.
476 Cassar, N., Wright, S. W., Thomson, P. G., Trull, W. T., Westwood, K. J., de Salas, M., Davidson,
477 A., Pearce, I., Davies, D. M., and Matear, R. J.: The relation of mixed-layer net community
478 production to phytoplankton community composition in the Southern Ocean, Global
479 Biogeochem. Cy., 29, 446-462, doi:10.1002/2014GB004936, 2015.
480 Chang, C.-H., Johnson, N. C., and Cassar, N.: Neural network-based estimates of Southern Ocean
481 net community production from in situ O_2/Ar and satellite observation: a methodological
482 study, Biogeosciences, 11, 3279-3297, doi:10.5194/bg-11-3279-2014, 2014.
483 Chen, B., Laws, E. A.: Is there a difference of temperature sensitivity between marine
484 phytoplankton and heterotrophs? Limnol. and Oceanogr., 62, 806-817,
485 doi:10.1002/lno.10462, 2017.

Cullen, J. J. and Lewis, M. R.: The kinetics of algal photoadaptation in the context of vertical mixing, J. Plankton Res., 10, 1039-1063, doi:10.1093/plankt/10.5.1039, 1988.

de Barr, J. W. H., Boyd, P. W., Coale, K. H., Landry M. R., Tsuda, A., Assmy, P., Bakker, D. C. E., Bozec, Y., Barber, R. T., Brzezinski, M. A., Buesseler, K. O., Boyé, M., Croot, P. L., Gervais, F., Gorbunov, M. Y., Harrison, P. J., Hiscock, W. T., Laan, P., Lancelot, C., Law, C. S., Levasseur, M., Marchetti, A., Millero, F. J., Nishioka, J., Nojiri, Y., van Oijen, T., Riebesell, U., Rijkenberg, M. J. A., Saito, H., Takeda, S., Timmermans, K. R., Veldhuis, M. J. W., Waite, A. M., and Wong, C. S.: Synthesis of iron fertilization experiments: From the Iron age in the Age of Enlightenment, J. Geophys. Res., 110, C09S16, doi:10.1029/2004JC002601, 2005.

Dunne, J. P., Armstrong, R. A., Gnanadesikan, A., and Sarmiento, J. L.: Empirical and mechanistic models for the particle export ratio, Global Biogeochem. Cy., 19, doi:10.1029/2004GB002390, 2005.

Duteil, O., Koeve, W., Oschlies, A., Bianchi, D., Galbraith, E., Kriest, I., and Matear, R.: A novel estimate of ocean oxygen utilisation points to a reduced rate of respiration in the ocean interior, Biogeosciences, 10, 7723-7738, doi:10.5194/bg-10-7723-2013, 2013.

Dutkiewicz, S., Follows, M., Marshall, J., and Gregg, W. W.: Interannual variability of phytoplankton abundances in the North Atlantic, Deep-Sea Res. Pt. II, 48, 2323-2344, doi:10.1016/S0967-0645(00)00178-8, 2001.

Edwards, K. F., Thomas, M. K., Klausmeier, C. A., and Litchman, E.: Phytoplankton growth and the interaction of light and temperature: A synthesis at the species and community level, Limnol. and Oceanogr., 61, 1232–1244, doi:10.1002/lno.10282, 2016.

Eppley, R. W.: Temperature and phytoplankton growth in the sea, Fishery Bulletin, 70, 1063-1085, 1972.

Eveleth, R., Cassar, N., Sherrell, R. M., Ducklow, H., Meredith, M., Venables, H., Lin, Y., and Li, Z.: Ice melt influence on summertime net community production along the Western Antarctic Peninsula, Deep-Sea Res. Pr. II, 139, 89-102, doi:10.1016/j.dsr2.2016.07.016, 2017.

Falkowski, P. G., Barber, R. T., and Smetacek, V.: Biogeochemical controls and feedbacks on ocean primary production, Science, 281, 200-206, doi:10.1126/science.281.5374.200, 1998.

517 Franks, P. J. S.: Has Sverdrup's critical depth hypothesis been tested? Mixed layers vs. turbulent
518 layers, ICES J. Mar. Sci., 72, 1897-1907, doi:10.1093/icesjms/fsu175, 2015.
519 Gong, X., Shi, J., Gao, H. W., and Yao, X. H.: Steady-state solutions for subsurface chlorophyll
520 maximum in stratified water columns with a bell-shaped vertical profile of chlorophyll,
521 Biogeosciences, 12, 905-919, doi:10.5194/bg-12-905-2015, 2015.
522 Gong, X., Jiang, W., Wang, L., Gao, H., Boss, E., Yao, X., Kao, S., and Shi, J.: Analytical solution
523 of the nitracline with the evolution of subsurface chlorophyll maximum in stratified water
524 columns, Biogeosciences, 14, 2371-2386, doi:10.5194/bg-14-2371-2017, 2017.
525 Gordon, H. R.: Can the Lambert-Beer law be applied to the diffuse attenuation coefficient of ocean
526 water? Limnol. and Oceanogr., 34, 1389-1409, doi:10.4319/lo.1989.34.8.1389, 1989.
527 Henson, S. A., Yool, A., and Sanders, R.: Variability in efficiency of particulate organic carbon
528 export: A model study, Global Biogeochem. Cy., 29, 33-45, doi:10.1002/2014GB004965,
529 2015.
530 Henson, S. A., Sanders, R., Madsen, E., Morris, P. J., Le Moigne, F., and Quartly, G. D.: A reduced
531 estimate of the strength of the ocean's biological carbon pump, Geophys. Res. Lett., 38,
532 L04606, doi:10.1029/2011GL046735, 2011.
533 Huang, K., Ducklow, H., Vernet, M., Cassar, N., and Bender, M. L.: Export production and its
534 regulating factors in the West Antarctica Peninsula region of the Southern Ocean, Global
535 Biogeochem. Cy., 26, GB2005, doi:10.1029/2010GB004028, 2012.
536 Huisman, J. and Weissing, F. J.: Light-limited growth and competition for light in well-mixed
537 aquatic environments: An elementary model, Ecology, 75, 507-520, doi:10.2307/1939554,
538 1994.
539 Huisman, J., van Oostveen, P., and Weissing, F. J.: Critical depth and critical turbulence: Two
540 different mechanisms for the development of phytoplankton blooms, Limnol. and
541 Oceanogr., 44, 1781-1787, doi:10.4319/lo.1999.44.7.1781, 1999.
542 Huisman, J., Thi, N. N. P., Karl, D. M., and Sommeijer B.: Reduced mixing generates oscillations
543 and chaos in the oceanic deep chlorophyll maximum, Nature, 439, 322-325,
544 doi:10.1038/nature04245, 2006.
545 Ito, T. and Follows, M. J.: Preformed phosphate, soft tissue pump and atmospheric CO_2, J. Mar.
546 Res., 63, 813-839, doi:10.1357/0022240054663231, 2005.

547 Jonsson, B. F., Doney, S. C., Dunne, J., and Bender, M.: Evaluation of the Southern Ocean O_2/Ar-
548 based NCP estimates in a model framework, J. Geophys. Res., 118, 385-399,
549 doi:10.1002/jgrg.20032, 2013.
550 Kremer, C. T., Thomas, M. K., and Litchman, E.: Temperature- and size-scaling of phytoplankton
551 population growth rates: Reconciling the Eppley curve and the metabolic theory of ecology,
552 Limnol. and Oceanogr., 62, 1658-1670, doi:10.1002/lno.10523, 2017.
553 Laws, E. A., Falkowski, P. G., Smith, W. O., Ducklow, H., and McCarthy, J. J.: Temperature
554 effects on export production in the open ocean, Global Biogeochem. Cy., 14, 1231-1246,
555 doi:10.1029/1999GB001229, 2000.
556 Lewis, M. R., Cullen, J. J., and Platt, T.: Relationships between vertical mixing and
557 photoadaptation of phytoplankton: Similarity criteria, Mar. Ecol. Prog. Ser., 15, 141-149,
558 doi:10.3354/meps015141, 1984.
559 Li, Z. and Cassar, N.: Satellite estimates of net community production based on O_2/Ar observations
560 and comparison to other estimates, Global Biogeochem. Cy., 30, 735-752,
561 doi:10.1002/2015GB005314, 2016.
562 Li, Z., Cassar, N., Huang, K., Ducklow, H., and Schofield, O.: Interannual variability in net
563 community production at the Western Antarctic Peninsula region (1997-2014), J. Geophys.
564 Res., 121, 4748-4762, doi:10.1002/2015JC011378, 2016.
565 López-Urrutia, A. and Morán, X. A. G.: Resource limitation of bacterial production distorts the
566 temperature dependence of oceanic carbon cycling, Ecology, 88, 817–822,
567 doi:10.1890/06-1641, 2007.
568 López-Urrutia, Á., San Martin, E., Harris, R. P., and Irigoien, X.: Scaling the metabolic balance
569 of the oceans, Proc. Natl Acad. Sci. USA, 103, 8739-8744, doi:10.1073/pnas.0601137103,
570 2006.
571 Maiti, K., Charette, M. A., Buesseler, K. O., and Kahru M.: An inverse relationship between
572 production and export efficiency in the Southern Ocean, Geophys. Res. Lett., 40, 1557-
573 1561, doi:10.1002/grl.50219, 2013.
574 Martin, J. H., Knauer, G. A., Karl, D. M., and Broenkow, W. W.: VERTEX: carbon cycling in the
575 northeast Pacific, Deep-Sea Res. Pr. A, 34, 267-285, doi:10.1016/0198-0149(87)90086-0,
576 1987.

577 Martin, P., Rutgers van der Loeff, M., Cassar, N., Vandromme, P., d'Ovidio, F., Stemman, L.,
578 Rengarajan, R., Soares, M., Gonzalez, H. E., Ebersbach, F., Lampitt, R., Sanders, R.,
579 Barnett, B., Smetacek, V., and Naqvi, S. W. A.: Iron fertilization enhanced net community
580 production but not downward particle flux during the Southern Ocean iron fertilization
581 experiment LOHAFEX, Global Biogeochem. Cy., 27, 871–881, doi:10.1002/gbc.20077,
582 2013.
583 Mitchell, B. G. and Holm-Hansen, O.: Observations and modeling of the Antarctic phytoplankton
584 crop in relation to mixing depth, Deep-Sea Res. Pr. A, 38, 981-1007, doi:10.1016/0198-
585 0149(91)90093-U, 1991.
586 Mitchell, B. G., Brody, E. A., Holm-Hansen, O., McClain, C., and Bishop, J.: Light limitation of
587 phytoplankton biomass and macronutrient utilization in the Southern Ocean, Limnol. and
588 Oceanogr., 36, 1662-1677, doi:10.4319/lo.1991.36.8.1662, 1991.
589 Morel, A. and Prieur, L.: Analysis of variations in ocean color, Limnol. and Oceanogr., 22, 709-
590 722, doi:10.4319/lo.1977.22.4.0709, 1977.
591 Mouw, C. B., Barnett, A., McKinley, G., Gloege, L., and Pilcher, D.: Global ocean particulate
592 organic carbon flux merged with satellite parameters, Earth Syst. Sci. Data, 8, 531-541,
593 doi:10.5194/essd-8-531-2016, 2016.
594 Nelson, D. M. and Smith, W. O.: Sverdrup revisited: Critical depths, maximum chlorophyll levels,
595 and the control of Southern Ocean productivity by the irradiance-mixing regime, Limnol.
596 and Oceanogr., 36, 1650-1661, doi:10.4319/lo.1991.36.8.1650, 1991.
597 Platt, T., Gallegos, C. L., and Harrison, W. G.: Photoinhibition of photosynthesis in natural
598 assemblages of marine phytoplankton, J. Mar. Res., 38, 687-701, 1980.
599 Rivkin, R. B. and Legendre, L.: Biogenic carbon cycling in the upper ocean: Effects of microbial
600 respiration, Science, 291, 2398-2400, doi:10.1126/science.291.5512.2398, 2001.
601 Sarmiento, J. L. and Gruber, N.: Ocean Biogeochemical Dynamics, Princeton University Press,
602 Princeton, New Jersey, 2006.
603 Shadwick, E. H., Tilbrook, B., Cassar, N., Trull, T. W., and Rintoul, S. R.: Summertime physical
604 and biological controls on O_2 and CO_2 in the Australian Sector of the Southern Ocean, J.
605 Marine Syst., 147, 21-28, doi:10.1016/j.jmarsys.2013.12.008, 2015.
606 Siegel, D. A., Buesseler, K. O., Behrenfeld, M. J., Benitez-Nelson, C. R., Boss, E., Brzezinski, M.
607 A., Burd, A., Carlson, C. A., D'Asaro, E. A., Doney, S. C., Perry, M. J., Stanley, R. H. R.,

608 and Steinberg, D. K.: Prediction of the export and fate of global ocean net primary
609 production: The exports science plan, Front. Mar. Sci., 3, doi:10.3389/fmars.2016.00022,
610 2016.
611 Sigman, D. M. and Boyle, E. A.: Glacial/interglacial variations in atmospheric carbon dioxide,
612 Nature, 407, 859-869, doi:10.1038/35038000, 2000.
613 Smetacek, V. and Passow, U.: Spring bloom initiation and Sverdrup's critical depth model, Limnol.
614 and Oceanogr., 35, 228–234, doi:10.4319/lo.1990.35.1.0228, 1990.
615 Smith, R. C. and Baker, K. S.: Optical classification of natural waters, Limnol. and Oceanogr., 23,
616 260-267, doi:10.4319/lo.1978.23.2.0260, 1978a.
617 Smith, R. C. and Baker, K. S.: The bio-optical state of ocean waters and remote sensing, Limnol.
618 and Oceanogr., 23, 247-259, doi:10.4319/lo.1978.23.2.0247, 1978b.
619 Stange, P., Bach, L. T., Le Moigne, F. A. C., Taucher, J., Boxhammer, T., and Riebesell, U.:
620 Quantifying the time lag between organic matter production and export in the surface ocean:
621 Implications for estimates of export efficiency, Geophys. Res. Lett., 44, 268-276,
622 doi:10.1002/2016GL07087, 2017.
623 Sunda, W. G. and Huntsman, S. A.: Interrelated influence of iron, light and cell size on marine
624 phytoplankton growth, Nature, 390, 389-392, doi:10.1038/37093, 1997.
625 Sverdrup, H. U., On conditions for the vernal blooming of phytoplankton, Journal du Conseil
626 International pour l'Exploration de la Mer, 18, 287-295, doi:10.1093/icesjms/18.3.287,
627 1953.
628 Taylor, J. R. and Ferrari, R.: Shutdown of turbulent convection as a new criterion for the onset of
629 spring phytoplankton blooms, Limnol. And Oceanogr., 56, 2293-
630 2307, doi:10.4319/lo.2011.56.6.2293, 2011.
631 Tortell, P. D., Bittig, H. C., Körtzinger, A., Jones, E. M., and Hoppema, M.: Biological and
632 physical controls on N_2, O_2, and CO_2 distributions in contrasting Southern Ocean surface
633 waters, Global Biogeochem. Cy., 29, 994-1013, doi:10.1002/2014GB004975, 2015.
634 Volk, T. and Hoffert, M. I.: Ocean carbon pumps: Analysis of relative strengths and efficiencies
635 in ocean-driven atmospheric CO_2 changes, in: The Carbon Cycle and Atmospheric CO_2:
636 Natural Variations Archean to Present, Geophys. Monogr. Ser., Vol. 32, edited by
637 Sundquist, E. T. and Broecker, W. S., AGU, Washington, D. C., 99-110, 1985.

638 Werdell, P. J. and Bailey, S. W.: An improved in-situ bio-optical data set for ocean color algorithm
639 development and satellite data product validation, Remote Sensing of Environment, 98,
640 122-140, doi:10.1016/j.rse.2005.07.001, 2005.
641 White, P. A., Kalff, J., Rasmussen, J. B., and Gasol, J. M.: The effect of temperature and algal
642 biomass on bacterial production and specific growth rate in fresh water and marine habitats,
643 Microb. Ecol., 21, 99-118, doi:10.1007/BF02539147, 1991.
644
645

Table 1. Model symbols, abbreviations, and units

Symbol	Description	Units
MLD	Mixed layer depth	m
$MLD_{C^*_{max}}$	Maximum MLD corresponds to maximum achievable autotroph's biomass concentration	m
z	Depth	m
Z_c	Critical depth	m
Z_p	Compensation depth	m
GPP(0,z)	Gross primary production	mmol C m^{-2} d^{-1}
NPP(z)	Net primary production at depth z	mmol C m^{-3} d^{-1}
NPP(0,z)	Net primary production above depth z	mmol C m^{-2} d^{-1}
NCP(z)	Net community production at depth z	mmol C m^{-3} d^{-1}
NCP(0,z)	Net community production above depth z	mmol C m^{-2} d^{-1}
HR(z)	Heterotrophic respiration at depth z	mmol C m^{-3} d^{-1}
HR(0,z)	Heterotrophic respiration above depth z	mmol C m^{-2} d^{-1}
NCP^*	The maximum NCP for a given MLD (upper bound on carbon export)	mmol C m^{-2} d^{-1}
NCP_B	NCP normalized to autotroph's biomass inventory in the mixed layer	d^{-1}
ef	Export ratio	unitless
f_{pt}	Ratio of satellite export production estimates to the upper bound on carbon export	unitless
N	Nutrient concentration	mmol m^{-3}
k_m^N	Half-saturation constant for nutrient concentration	mmol m^{-3}
N_m	Nutrient effect on phytoplankton growth $N_m = \frac{N}{N+k_m^N}$	unitless
PAR	Photosynthetically active radiation	Einstein m^{-2} d^{-1}
I_0	Photosynthetically active radiation just beneath water surface	Einstein m^{-2} d^{-1}
$I(z)$	Photosynthetically active radiation at depth z	Einstein m^{-2} d^{-1}
k_m^I	Half-saturation constant for irradiance	Einstein m^{-2} d^{-1}
$I_m(z)$	Light effect on phytoplankton growth at depth z, $I_m(z) = \frac{I(z)}{I(z)+k_m^I} = \frac{I_0 \times e^{-K_I \times z}}{I_0 \times e^{-K_I \times z}+k_m^I}$	unitless
$I_m(0,z)$	Integrated light effect on phytoplankton growth above depth z, $I_m(0,z) = -\frac{1}{K_I} \times ln\left(\frac{I_0 \times e^{-K_I \times z}+k_m^I}{I_0+k_m^I}\right)$	unitless
PAR_{ML}	Average PAR in the mixed layer ($PAR_{ML} = \frac{1-e^{-K_I \times MLD}}{K_I \times MLD} \times I_0$)	Einstein m^{-2} d^{-1}
μ	Phytoplankton growth rate	d^{-1}
μ_{max}	Maximum phytoplankton growth rate	d^{-1}

μ_{max}^{0}	Maximum phytoplankton growth rate for $T = 0$ °C	d^{-1}
r_{HR}	Heterotrophic respiration ratio	d^{-1}
r_{HR}^{0}	Heterotrophic respiration ratio for $T = 0$ °C	d^{-1}
K_I	Light attenuation coefficient ($K_I = K_I^w + K_I^{nw}$)	m^{-1}
K_I^w	Light attenuation coefficient due to water	m^{-1}
K_I^{nw}	Light attenuation coefficient due to optically active components	m^{-1}
k_c	Specific attenuation coefficient for irradiance	$m^2\ mmol^{-1}$
C	Phytoplankton biomass concentration	$mmol\ m^{-3}$
C^*	Phytoplankton biomass concentration that maximizes NCP	$mmol\ m^{-3}$
C_{max}^*	Maximum achievable autotroph's biomass concentration	$mmol\ m^{-3}$
POC	Particulate organic carbon	$mmol\ m^{-3}$
DOC	Dissolved organic carbon	$mmol\ m^{-3}$
CDOM	Colored dissolved organic matter	m^{-1}
NAP	Non-algal particles	$mmol\ m^{-3}$
T	Temperature	°C
P_t	Temperature dependence for phytoplankton growth rate	$°C^{-1}$
B_t	Temperature dependence for heterotrophic respiration ratio	$°C^{-1}$
CO_2	Carbon dioxide	ppmv

Table 2. Value or range of values with references for the parameters used in the model.

Parameter	**Range or value**	**Reference**
K_I^w	0.09	(Werdell and Bailey, 2005)
k_c	0.03	(Werdell and Bailey, 2005)
Carbon to chlorophyll ratio	90	(Arrigo et al., 2008)
k_m^I	4.1 Einstein m^{-2} d^{-1}	(Behrenfeld and Falkowski, 1997)
P_t	0.0663	(Eppley, 1972)
B_t	0.08	(Rivkin and Legendre, 2001; López-Urrutia et al., 2006)
μ_{max}	1 d^{-1}, 1.2 d^{-1}	(Laws et al., 2000; Eppley, 1972)
r_{HR}	0.1 d^{-1}, 0.2 d^{-1}	(Laws et al., 2000; Mitchell et al., 1991)

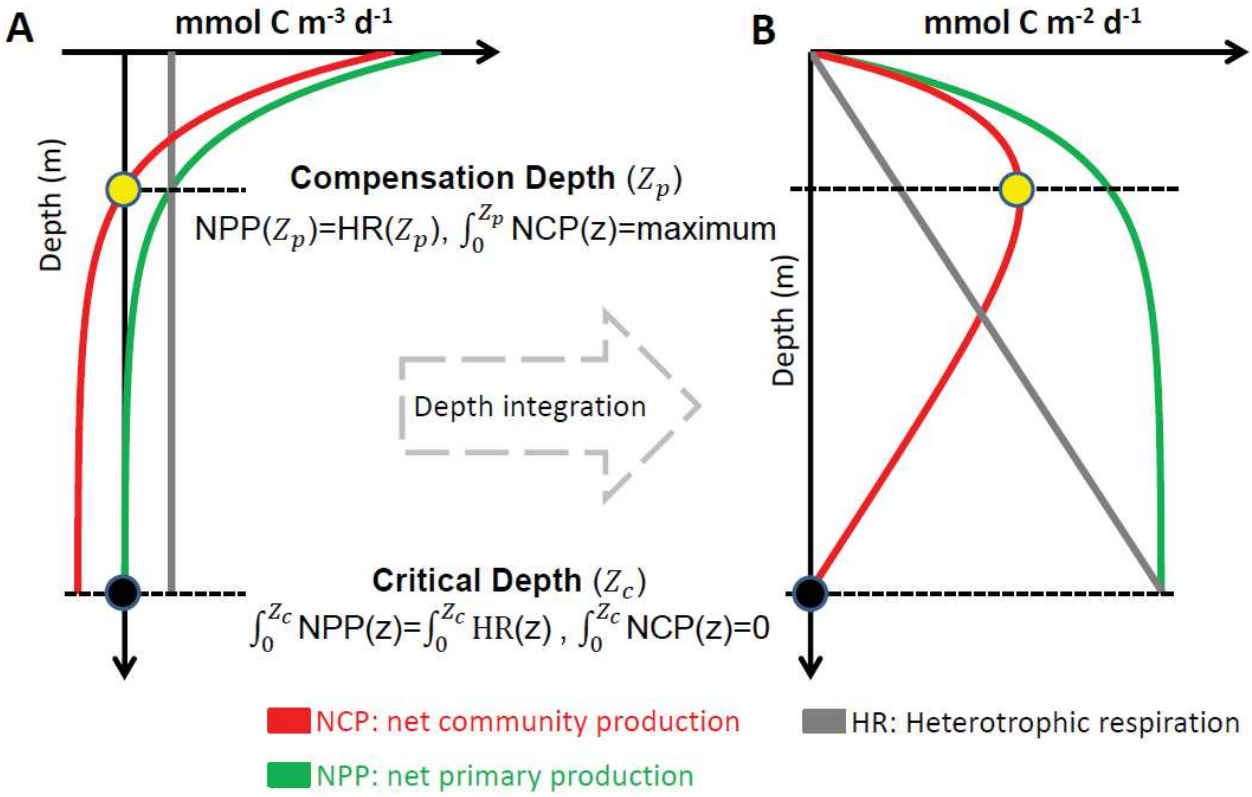

Figure 1. Schematic diagram of depth-profiles of net community production (NCP), net primary production (NPP), and heterotrophic respiration (HR). Yellow and black dots represent the compensation and critical depths, respectively.

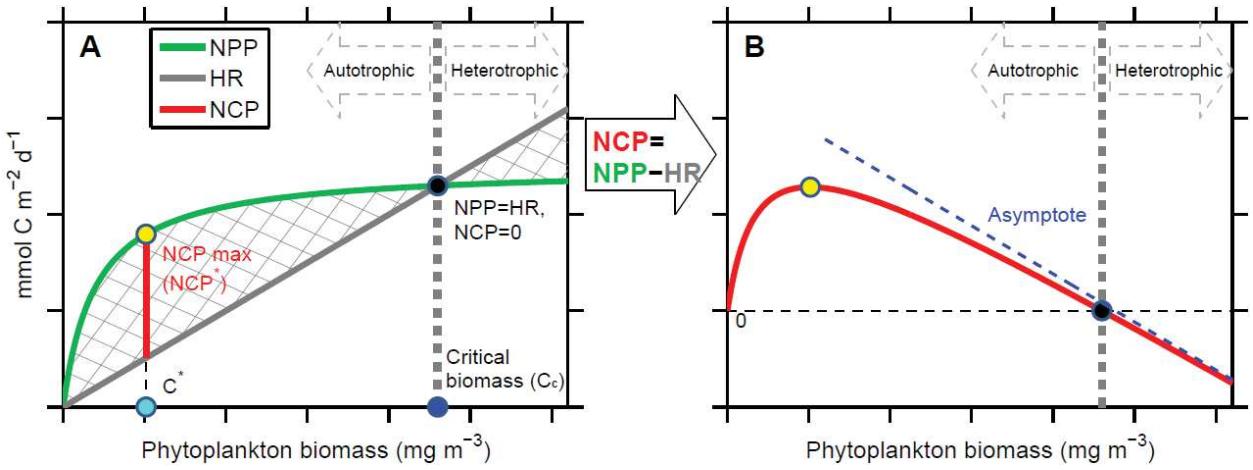

Figure 2. Relationship between net primary production (NPP), heterotrophic respiration (HR), net community production (NCP), and phytoplankton biomass concentration (C) for a given mixed layer depth (MLD). Hatched area in panel A represents NCP. The yellow dot represents the maximal NCP (NCP*) obtainable for a given MLD, with the corresponding phytoplankton biomass concentration (C*) denoted with a cyan dot. NCP on the right of the yellow dot decreases with C due to self-shading. Black dot represents depth-integrated NCP =0 (i.e., NPP=HR), with the corresponding phytoplankton biomass concentration defined as critical biomass (C_c) and denoted with a blue dot. Ecosystems on the left and right of this threshold are net autotrophic and heterotrophic, respectively. The asymptote (dashed blue line) in panel B represents a system dominated by heterotrophic respiration (i.e., NCP ≈ HR >> NPP).

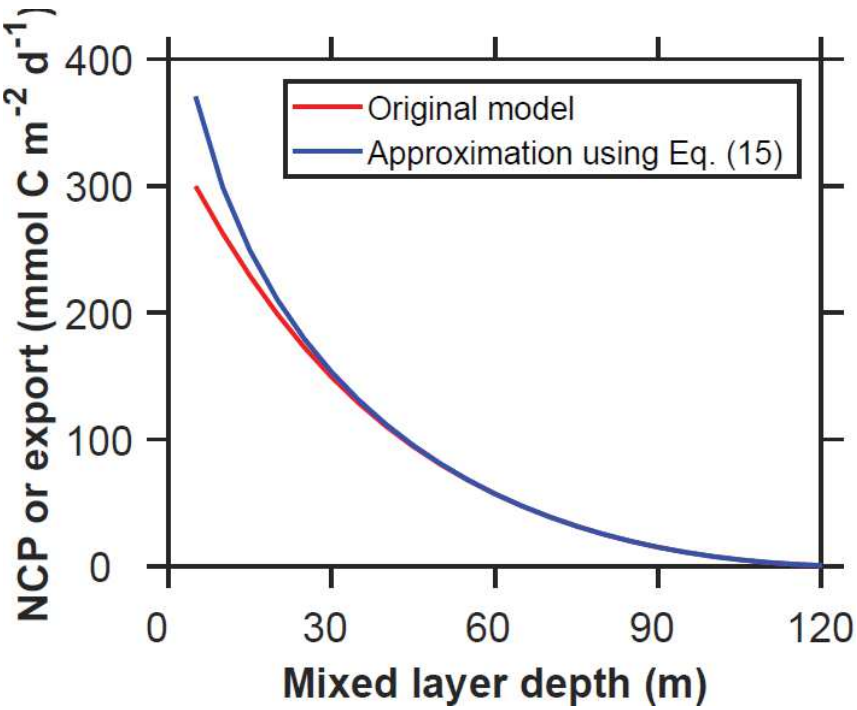

Figure 3. Upper bounds derived using the original and approximated models. The upper bound for the original model (equations (8-10)) is estimated through a non-linear optimization approach. The upper bound for the approximated model is calculated analytically from equation (19). The models use the constants listed in Table 2 and $I_m(0) = 0.9$. Decreasing $I_m(0)$ and increasing r_{HR} results in greater discrepancies between the original and approximated models in regions with shallow mixed layers.

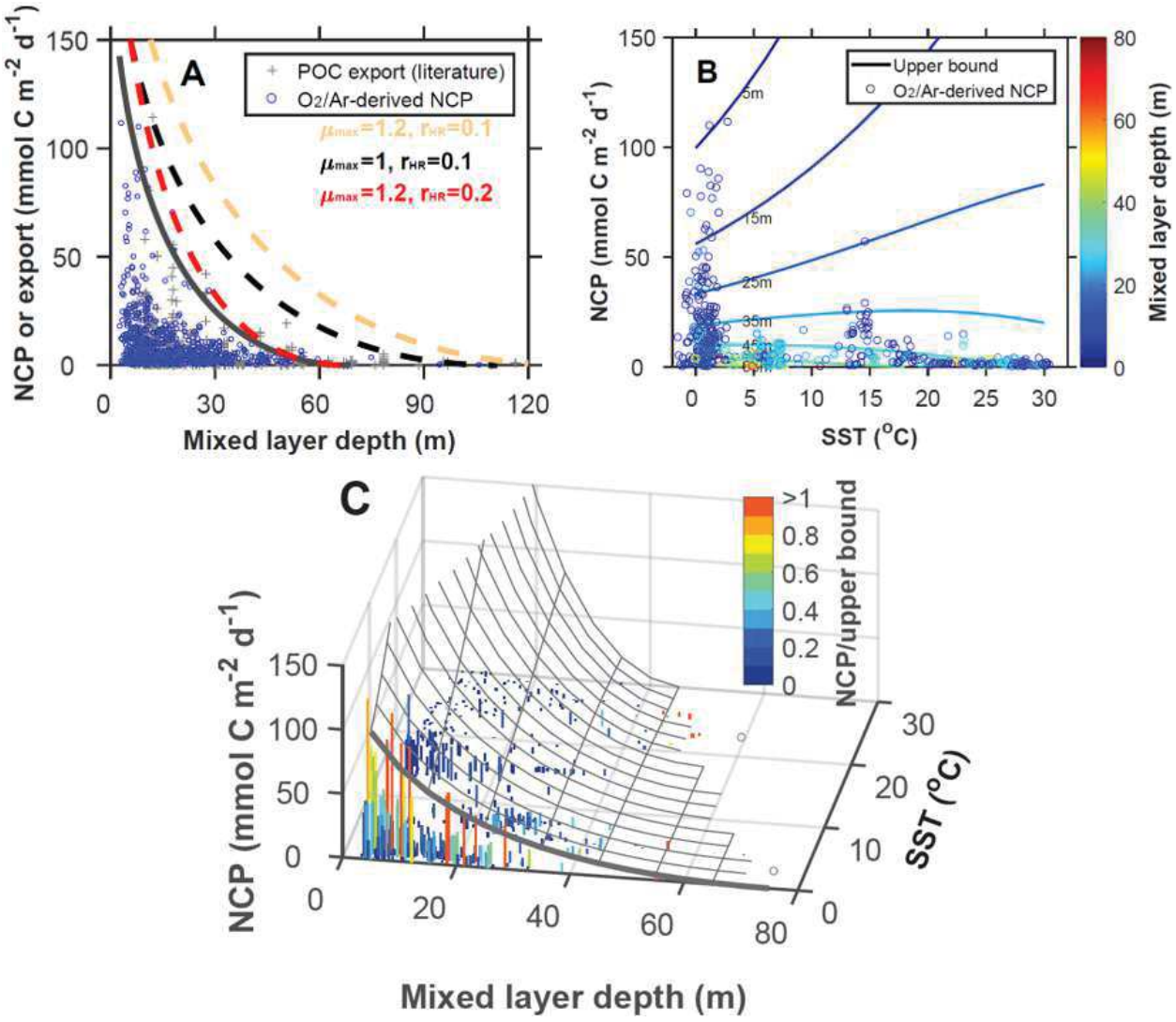

Figure 4. Modeled upper bound on carbon export production compared to field observations as a function of mixed layer depth (MLD) and sea surface temperature (SST). (A) The thick gray line represents the upper bound fitted to the net community production (NCP) data. Dash-lines represent the upper bounds calculated using parameters available in the literature (Table 2). (B) NCP as a function of SST with isopleths of constant upper bounds color coded for MLD. NCP observations are color coded with MLD. (C) Surface representing the envelope of the modeled upper bound of carbon export production as a function of SST and MLD. Bars represent field observations color coded with the ratio of NCP to the upper bound. Observations are based on

^{234}Th and sediment traps estimates of carbon export production and O_2/Ar-derived NCP. A stoichiometric ratio of O_2/C=1.4 was used to convert NCP from O_2 to C units (Laws, 1991). To account for the effect of PAR on export production, both MLD and carbon fluxes are normalized to $-log(1 - I_m(0))$ (see equations (19) and (21)). The temperature dependence of r_{HR} was modeled as $r_{HR} = r_{HR}^0 \times e^{0.08 \times T}$.

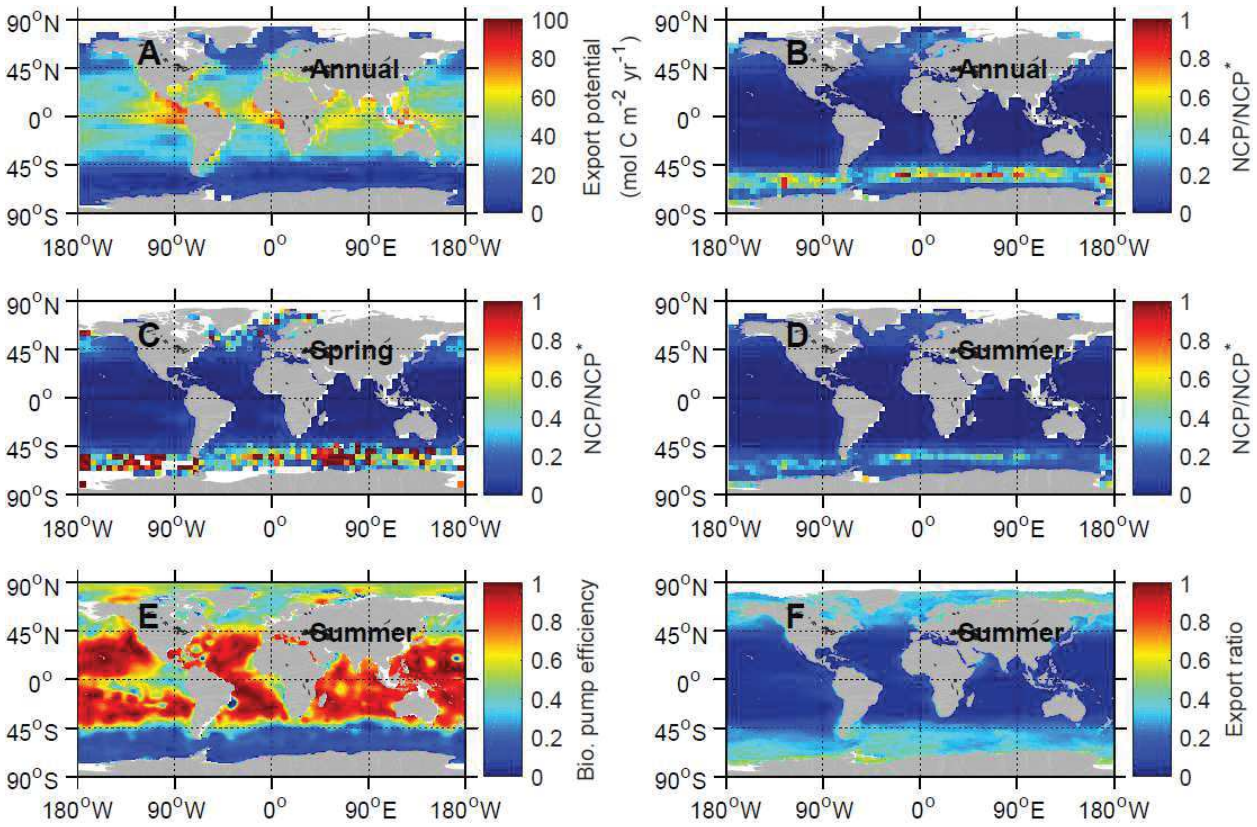

Figure 5. (A) Modeled upper bound on carbon export derived from equation (19), (B-D) ratios of satellite export production estimates to the upper bound on carbon export, (E) biological pump efficiency calculated as the difference in nutrient concentrations between surface and depth, normalized to nutrient concentrations at depth (Sarmiento and Gruber, 2006) (nitrate concentration from World Ocean Atlas (https://www.nodc.noaa.gov/OC5/woa13/)), and (F) export ratio derived from Dunne et al. (2005). Annual represents annually-integrated value. Spring and summer represent average value in spring and summer, respectively. In the northern hemisphere, spring and summer seasons are defined as March-May and June-August, respectively. In the southern hemisphere, spring and summer seasons are defined as September-November and December-February, respectively.

Supplementary for: **A mechanistic model of an upper bound on oceanic carbon export as a function of mixed layer depth and temperature**

Zuchuan Li*, Nicolas Cassar

Division of Earth and Ocean Sciences, Nicholas School of the Environment, Duke University, Durham, North Carolina, USA

* Corresponding to: zuchuan.li@duke.edu

1. Derivation of first and second derivatives of $NCP(0, MLD)$

To explore how $NCP(0, MLD)$ varies with C, we calculate its first and second derivatives with respect to C. Based on equations (8-10):

$$\frac{dNCP(0,MLD)}{dC}$$

$$= \frac{d\left\{-N_m \times \mu_{max} \times \frac{ln\left(\frac{I_0 \times e^{-K_I \times MLD} + k_m^I}{I_0 + k_m^I}\right) \times C}{K_I}\right\}}{dC} - \frac{d\{r_{HR} \times C \times MLD\}}{dC}$$

$$= -N_m \times \mu_{max}$$

$$\times \frac{\left\{ln\left(\frac{I_0 \times e^{-K_I \times MLD} + k_m^I}{I_0 + k_m^I}\right) - C \times \frac{I_0 + k_m^I}{I_0 \times e^{-K_I \times MLD} + k_m^I} \times \frac{I_0 \times e^{-K_I \times MLD}}{I_0 + k_m^I} \times k_c \times MLD\right\} \times K_I - k_c \times C \times ln\left(\frac{I_0 \times e^{-K_I \times MLD} + k_m^I}{I_0 + k_m^I}\right)}{{K_I}^2}$$

$$- r_{HR} \times MLD$$

$$= -N_m \times \mu_{max} \times \frac{\{-K_I \times I_m(0,MLD) - C \times I_m(MLD) \times k_c \times MLD\} \times K_I + k_c \times C \times K_I \times I_m(0,MLD)}{{K_I}^2} - r_{HR} \times MLD$$

$$= N_m \times \mu_{max} \times \frac{K_I \times I_m(0,MLD) + k_c \times C \times I_m(MLD) \times MLD - k_c \times C \times I_m(0,MLD)}{K_I} - r_{HR} \times MLD$$

$$= N_m \times \mu_{max} \times \frac{K_I \times I_m(0,MLD) - k_c \times C \times I_m(0,MLD) + k_c \times C \times MLD \times I_m(MLD)}{K_I} - r_{HR} \times MLD$$

$$= N_m \times \mu_{max} \times \frac{K_I^w \times I_m(0,MLD) + k_c \times C \times MLD \times I_m(MLD)}{K_I^w + k_c \times C} - r_{HR} \times MLD \qquad (S1)$$

where $I_m(MLD) = \frac{I_0 \times e^{-K_I \times MLD}}{I_0 \times e^{-K_I \times MLD} + k_m^I}$.

Based on equation (S1), the second derivative of $NCP(0, MLD)$ in equation (8) with respect to C may be expressed as follows:

$$\frac{d^2NCP(0,MLD)}{dC^2} = N_m \times \mu_{max} \times \left\{\frac{dy}{dC} + \frac{dg}{dC}\right\} \qquad (S2)$$

where $y = \frac{K_I^w \times I_m(0,MLD)}{K_I} = -\frac{K_I^w \times ln\left(\frac{I_0 \times e^{-K_I \times MLD} + k_m^I}{I_0 + k_m^I}\right)}{{K_I}^2}$ and $g = \frac{k_c \times C \times MLD \times I_m(MLD)}{K_I}$.

$\frac{dy}{dC}$ and $\frac{dg}{dC}$ are derived as follows:

$$\frac{dy}{dC} = -K_I^w \times \frac{\frac{I_0 + k_m^I}{I_0 \times e^{-K_I \times MLD} + k_m^I} \times \frac{I_0 \times e^{-K_I \times MLD}}{I_0 + k_m^I} \times (-k_c \times MLD) \times {K_I}^2 - ln\left(\frac{I_0 \times e^{-K_I \times MLD} + k_m^I}{I_0 + k_m^I}\right) \times 2 \times K_I \times k_c}{{K_I}^4}$$

$$= -K_I^w \times \frac{-I_m(MLD) \times MLD \times {K_I}^2 + I_m(0, MLD) \times 2 \times {K_I}^2}{{K_I}^4} \times k_c$$

$$= K_I^w \times \frac{I_m(MLD) \times MLD - 2 \times I_m(0, MLD)}{{K_I}^2} \times k_c \qquad (S3)$$

$$\frac{dg}{dC}$$

$$= \frac{-k_c \times C \times MLD \times I_m(MLD) \times k_c + k_c \times MLD \times I_m(MLD) \times K_I}{{K_I}^2}$$

$$+ \frac{k_c \times C \times MLD \times \frac{I_0 \times e^{-K_I \times MLD} \times (-k_c \times MLD) \times \{I_0 \times e^{-K_I \times MLD} + k_m^I\} - I_0 \times e^{-K_I \times MLD} \times I_0 \times e^{-K_I \times MLD} \times (-k_c \times MLD)}{\{I_0 \times e^{-K_I \times MLD} + k_m^I\}^2} \times K_I}{{K_I}^2}$$

$$= \frac{k_c \times MLD \times I_m(MLD) \times K_I + k_c \times C \times MLD \times \frac{I_0 \times e^{-K_I \times MLD} \times (-k_c \times MLD) \times k_m^I}{\{I_0 \times e^{-K_I \times MLD} + k_m^I\}^2} \times K_I - {k_c}^2 \times C \times MLD \times I_m(MLD)}{{K_I}^2}$$

$$= \frac{k_c \times MLD \times I_m(MLD) \times K_I + k_c \times C \times MLD \times \frac{I_m(MLD)^2 \times (-k_c \times MLD) \times k_m^I}{I_0 \times e^{-K_I \times MLD}} \times K_I - {k_c}^2 \times C \times MLD \times I_m(MLD)}{{K_I}^2}$$

$$= \frac{MLD \times I_m(MLD) \times K_I + k_c \times C \times MLD \times \frac{-I_m(MLD)^2 \times MLD \times k_m^I}{I_0 \times e^{-K_I \times MLD}} \times K_I - k_c \times C \times MLD \times I_m(MLD)}{{K_I}^2} \times k_c$$

$$= \frac{MLD \times I_m(MLD) \times K_I - k_c \times C \times MLD \times I_m(MLD)}{{K_I}^2} \times k_c - \frac{k_c \times C \times MLD \times \frac{I_m(MLD)^2 \times MLD \times k_m^I}{I_0 \times e^{-K_I \times MLD}} \times K_I}{{K_I}^2} \times k_c$$

$$= \frac{MLD \times I_m(MLD) \times K_I^w}{{K_I}^2} \times k_c - \frac{MLD^2 \times C \times I_m(MLD)^2 \times k_m^I}{K_I \times I_0 \times e^{-K_I \times MLD}} \times {k_c}^2 \quad (S4)$$

Substituting equations (S3-S4) into equation (S2) yields:

$$\frac{d^2 NCP(0, MLD)}{dC^2}$$

$$= N_m \times \mu_{max} \times \left\{K_I^w \times \frac{I_m(MLD) \times MLD - 2 \times I_m(0, MLD)}{{K_I}^2} \times k_c + \frac{MLD \times I_m(MLD) \times K_I^w}{{K_I}^2} \times k_c - \frac{MLD^2 \times C \times I_m(MLD)^2 \times k_m^I}{K_I \times I_0 \times e^{-K_I \times MLD}} \times {k_c}^2\right\}$$

$$= N_m \times \frac{\mu_{max}}{K_I} \times k_c \times \left\{\frac{2 \times K_I^w}{K_I} \times \left(I_m(MLD) \times MLD - I_m(0, MLD)\right) - \frac{MLD^2 \times C \times I_m(MLD)^2 \times k_m^I}{I_0 \times e^{-K_I \times MLD}} \times k_c\right\} \qquad (S5)$$

2. NCP upper bound for shallow MLD

When $0 \le MLD < MLD_{C^*_{max}}$ and $MLD \to 0$, $1 - \exp(-K_I \times MLD)$ in equation (15) can be approximated using a second order of Taylor expansion:

$$1 - \exp(-K_I \times MLD) \approx K_I \times MLD - \frac{1}{2} \times (K_I \times MLD)^2 \qquad (S6)$$

From equation (S6), we may approximate equation (15):

$$NCP(0, MLD) = C \times MLD \times \left(-\frac{1}{2} \times K_I \times MLD \times \mu^* + \mu^* - r_{HR}\right) \qquad (S7)$$

where the first derivative of equation (S7) with respective to C is:

$$\frac{dNCP(0, MLD)}{dC} = MLD \times \left(-K_I^{nw} \times MLD \times \mu^* - \frac{1}{2} \times K_I^w \times MLD \times \mu^* + \mu^* - r_{HR}\right) \qquad (S8)$$

when $0 \le MLD < MLD_{C^*_{max}}$, K_I^{nw} should satisfy $K_I^{nw} \le k_c \times C^*_{max} < -\frac{1}{2} \times K_I^w + \frac{\mu^* - r_{HR}}{\mu^*} \times \frac{1}{MLD}$, and equation (S8) should be greater than 0. $NCP(0, MLD)$ thus increases with C in the range of $0 \le MLD < MLD_{C^*_{max}}$, with an upper bound obtained at C^*_{max}:

$$NCP^* = \mu^* \times C^*_{max} \times MLD \times \left(-\frac{1}{2} \times (k_c \times C^*_{max} + K_I^w) \times MLD + \frac{\mu^* - r_{HR}}{\mu^*}\right) \qquad (S9)$$

Over this range, Equation (S9) states that NCP^* increases with MLD, and as expected is nil when MLD equals 0.

3. An upper bound on export ratio

The export ratio ef (equation (24)) is written as follows:

$$ef = \frac{NCP(0, MLD)}{NPP(0, MLD)} = 1 - \frac{K_I \times MLD}{-ln\left(\frac{I_0 \times e^{-K_I \times MLD} + k_m^I}{I_0 + k_m^I}\right)} \times \frac{1}{N_m} \times \frac{r_{HR}}{\mu_{max}} \qquad (S10)$$

The first derivative of ef with respect to C is expressed as:

$$\frac{\partial ef}{\partial C} = -\left(1 - \frac{MLD \times I_m(MLD)}{I_m(0, MLD)}\right) \times \frac{1}{K_I} \times k_c \times (1 - ef) \qquad (S11)$$

According to the inequality in equation (13), $\frac{\partial ef}{\partial C}$ in equation (S11) must be less than zero. Therefore, ef maximizes when $C \to 0$ ($ef = 1 - \frac{1}{I_m(0)} \times \frac{1}{N_m} \times \frac{r_{HR}}{\mu_{max}}$). Considering that the minimum values for the terms $\frac{1}{N_m}$

and $\frac{1}{I_m(0)}$ are 1, ef is maximized in equation (S10) with $ef^* = 1 - \frac{r_{HR}}{\mu_{max}} = 1 - \alpha \times e^{(B_T - P_T)\times T}$, where α represents an constant, $B_T = 0.11$ and $P_T = 0.0633$ for the equation (5) of Cael and Follows (2016).

4. Dataset

To test the performance of our upper bound model, we compiled observations of net community production (Table S1) and carbon export in the world's oceans.

4.1 O_2/Ar Net Community Production

The O_2/Ar method estimates NCP through a mass balance of biological O_2 in the mixed layer. Because Ar and O_2 have similar temperature dependencies and solubilities (Craig and Hayward, 1987), the saturation state of their ratio can partition oxygen concentration due to physical ($[O_2]_{phys}$) and biological processes ($[O_2]_{\mathrm{biol}}$) (Cassar et al., 2011):

$$[\mathrm{O_2}]_{\mathrm{biol}} = [\mathrm{O_2}] - [\mathrm{O_2}]_{\mathrm{phys}} \approx [\mathrm{O_2}] - \frac{[\mathrm{Ar}]}{[\mathrm{Ar}]_{\mathrm{sat}}}[\mathrm{O_2}]_{\mathrm{sat}} = \frac{[\mathrm{Ar}]}{[\mathrm{Ar}]_{\mathrm{sat}}}[\mathrm{O_2}]_{\mathrm{sat}}\Delta(\mathrm{O_2/Ar}) \qquad (S12)$$

where $\Delta(\mathrm{O_2/Ar}) = \left[\frac{([\mathrm{O_2}]/[\mathrm{Ar}])}{([\mathrm{O_2}]/[\mathrm{Ar}])_{\mathrm{sat}}} - 1\right]$ is the biological O_2 supersatulation. When ignoring vertical mixing and lateral advection, we can write the mass balance for $[\mathrm{O_2}]_{\mathrm{biol}}$ in the mixed layer as follows (Cassar et al., 2011):

$$MLD\frac{d[O_2]_{biol}}{dt} = NCP - k_{\mathrm{O_2}}\frac{[\mathrm{Ar}]}{[\mathrm{Ar}]_{\mathrm{sat}}}[\mathrm{O_2}]_{\mathrm{sat}}\Delta(\mathrm{O_2/Ar}) \qquad (S13)$$

where $k_{\mathrm{O_2}}$ is the gas exchange velocity for O_2. At steady state (i.e., $\frac{d[O_2]_{biol}}{dt} = 0$), equation (S13) reduces to (Cassar et al., 2011; Reuer et al., 2007):

$$\mathrm{NCP} = k_{\mathrm{O_2}}[\mathrm{O_2}]_{\mathrm{sat}}\Delta(\mathrm{O_2/Ar}) \qquad (S14)$$

where $\frac{[\mathrm{Ar}]}{[\mathrm{Ar}]_{\mathrm{sat}}}$ in equation (S13) is assumed to equal 1, which introduces an error of up to a couple percent in NCP estimates under most conditions (Cassar et al., 2011; Eveleth et al., 2014).

To derive NCP using equation (S14), we calculate $k_{\mathrm{O_2}}$ using daily NCEP wind speeds, MLD, the parameterization of Wanninkhof (1992), and a weighting technique to account for wind speed history following (Reuer et al., 2007). Uncertainties and biases in O_2/Ar NCP estimates can be found in previous studies (Bender et al., 2011; Cassar et al., 2014; Jonsson et al., 2013).

Table S1. O_2/Ar measurements included in this study.

Citation	Cruise	Start date	End date	Location
(Reuer et al., 2007)	A0103	10/30/2001	12/10/2001	South of Australia
	SOFEXR	01/07/2002	02/12/2002	South of New Zealand
	SOFEXM	01/20/2002	02/24/2002	South of New Zealand
	NBP0305	10/28/2003	11/13/2003	South of New Zealand
	ANTXXI/2	11/18/2003	01/15/2004	South of South Africa
	NBP0305A	12/20/2003	12/29/2003	South of New Zealand
(Cassar et al., 2007)	AA2006	12/03/2005	02/09/2006	South of Australia
(Juranek et al., 2010)	AMT16	05/22/2005	06/28/2005	Atlantic
	AMT17	10/18/2005	11/25/2005	Atlantic
(Stanley et al., 2010)	EUC-Fe	07/19/2006	08/31/2006	Equatorial Pacific
(Tortell et al., 2011)	CORSACS II	11/03/2006	12/11/2006	South of New Zealand
(Cassar et al., 2011)	SAZ-SENSE	01/19/2007	02/19/2007	South of Australia
(Huang et al., 2012)	LMG0801	01/07/2008	01/29/2008	Drake Passage
(Hamme et al., 2012)	GASEX	03/02/2008	04/11/2008	South of Atlantic
(Martin et al., 2013)	LOHAFEX	01/26/2009	03/06/2009	South of Atlantic
(Shadwick et al., 2015)	AA1203	01/08/2012	02/10/2012	South of Australia
(Eveleth et al., 2016)	LMG1201	12/30/2011	02/07/2012	Drake Passage
	LMG1301	01/05/2013	02/03/2013	Drake Passage
	LMG1401	01/01/2014	02/01/2014	Drake Passage
(Huang et al., unpublished)	LMG0901	01/06/2009	02/01/2009	Drake Passage
	LMG1001	01/01/2010	02/07/2010	Drake Passage
	LMG1101	01/02/2011	02/06/2011	Drake Passage

4.2 Sediment trap and ^{234}Thorium POC export production

We also compared NCP^* to sediment-trap and ^{234}Th-derived POC export production estimates from the dataset recently compiled by Mouw et al. (2016). These observations were adjusted to reflect a flux at the base of the mixed layer using the Martin curve with $b = -0.86$ (Martin et al., 1987). Monthly climatological MLD were used.

4.3 Mixed layer depth

We derived MLD using Argo temperature-salinity profiling floats which were downloaded from http://www.usgodae.org/. As real-time data (after 2008) have not been thoroughly checked, we only used profiles with temperature, salinity, and pressure with a quality flag of '1' ('good data') or '2' ('probably good data'). To improve coverage, we also used the temperature and salinity profiles obtained by CTD casts in the World Ocean Database. These profiles were downloaded from the National Oceanographic Data Center (NODC) https://www.nodc.noaa.gov/access/index.html.

MLD is estimated as the depth at which the potential density (σ_θ) exceeds a near-surface reference value at 10 m depth by $\Delta\sigma_\theta = 0.03$ kg m^{-3} (de Boyer Montegut et al., 2004; Dong et al., 2008). Estimates were averaged to daily $5° \times 5°$ grids, from which monthly climatologies were calculated (Figure S1).

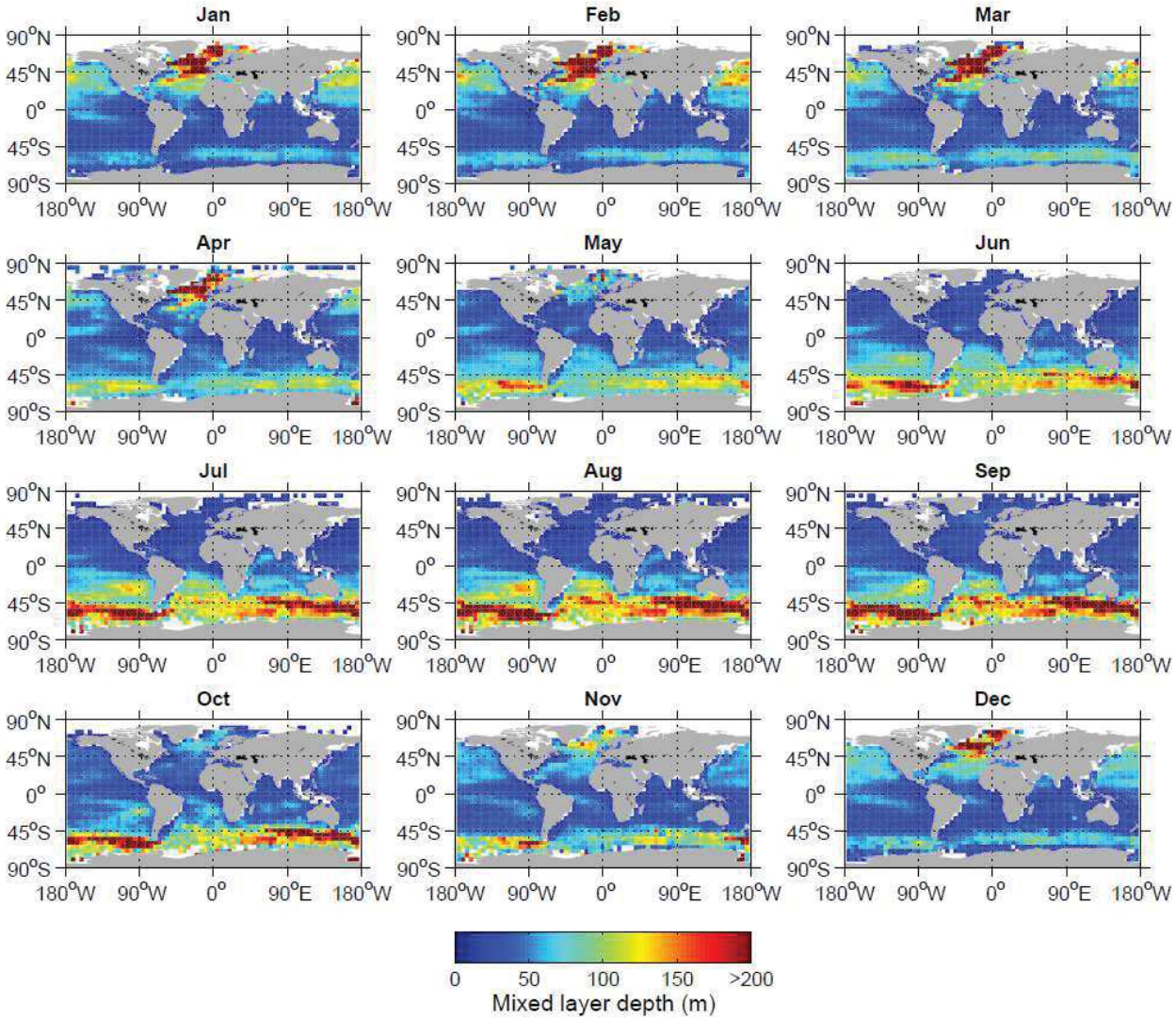

Figure S1. Climatology of monthly mixed layer depth.

4.4 Satellite properties

To derive a global distribution of NCP^*, we used monthly SST and PAR climatologies calculated based on MODIS-Aqua observations from 2002-2015 with a spatial resolution of $0.083° \times 0.083°$ (downloaded from NASA's ocean color website (http://oceancolor.gsfc.nasa.gov/cms/)). We compared $NCP^*$to monthly and annual NCP climatologies as simulated by the algorithms developed by Li and Cassar (2016). This NCP dataset represents the average of 11 satellite algorithms of export production for observations from 1997 to 2010 (Figure S2). More details can be found in Li and Cassar (2016).

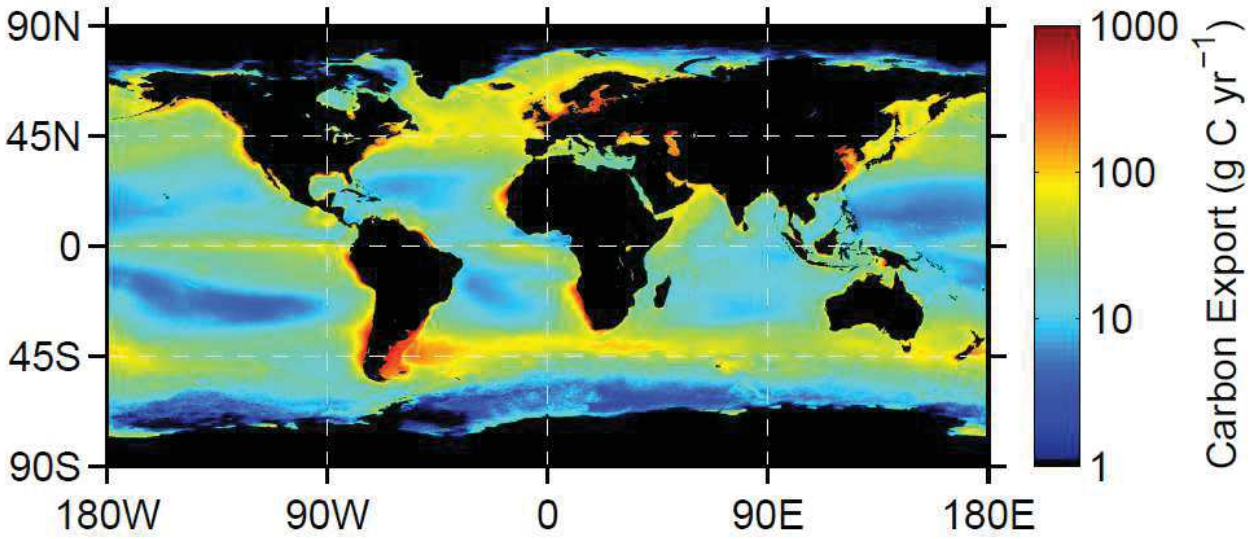

Figure 2S. Average annual export production derived using 11 algorithms (see Li and Cassar (2016)).

4.5. Diffusion attenuation coefficient for photosynthetically active radiation

Constants k_c and K_I^w in equation (10) were derived using the NOMAD dataset (Werdell and Bailey, 2005), which includes chlorophyll a concentration and K_I (Figure S3). NOMAD was downloaded from https://seabass.gsfc.nasa.gov/wiki/NOMAD. The regression in Figure S3 was converted to equation (10) using a carbon to chlorophyll ratio of 90 (Arrigo et al., 2008).

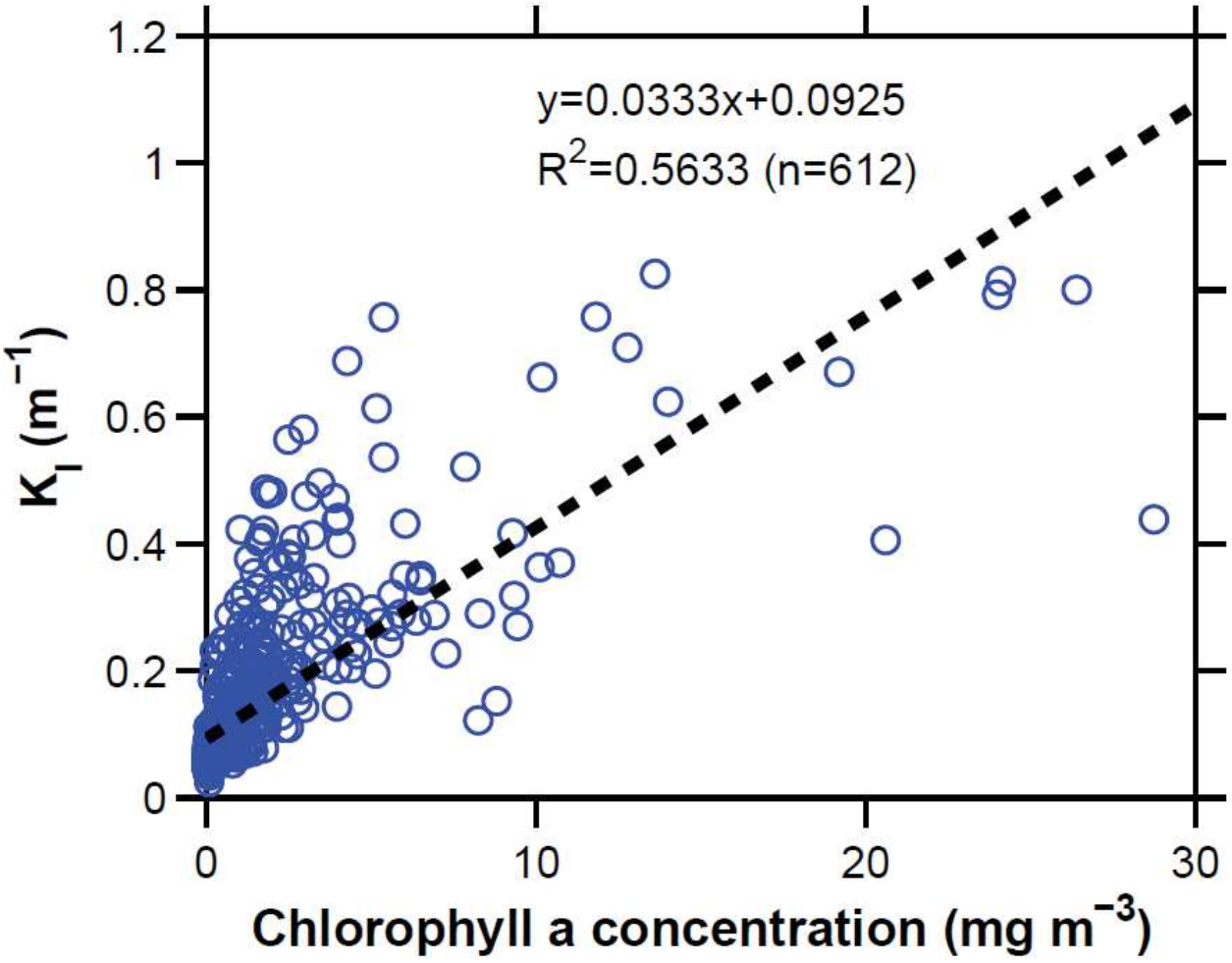

Figure S3. Attenuation coefficient for photosynthetically active radiation (PAR) as a function of chlorophyll a concentration based on the NOMAD dataset.

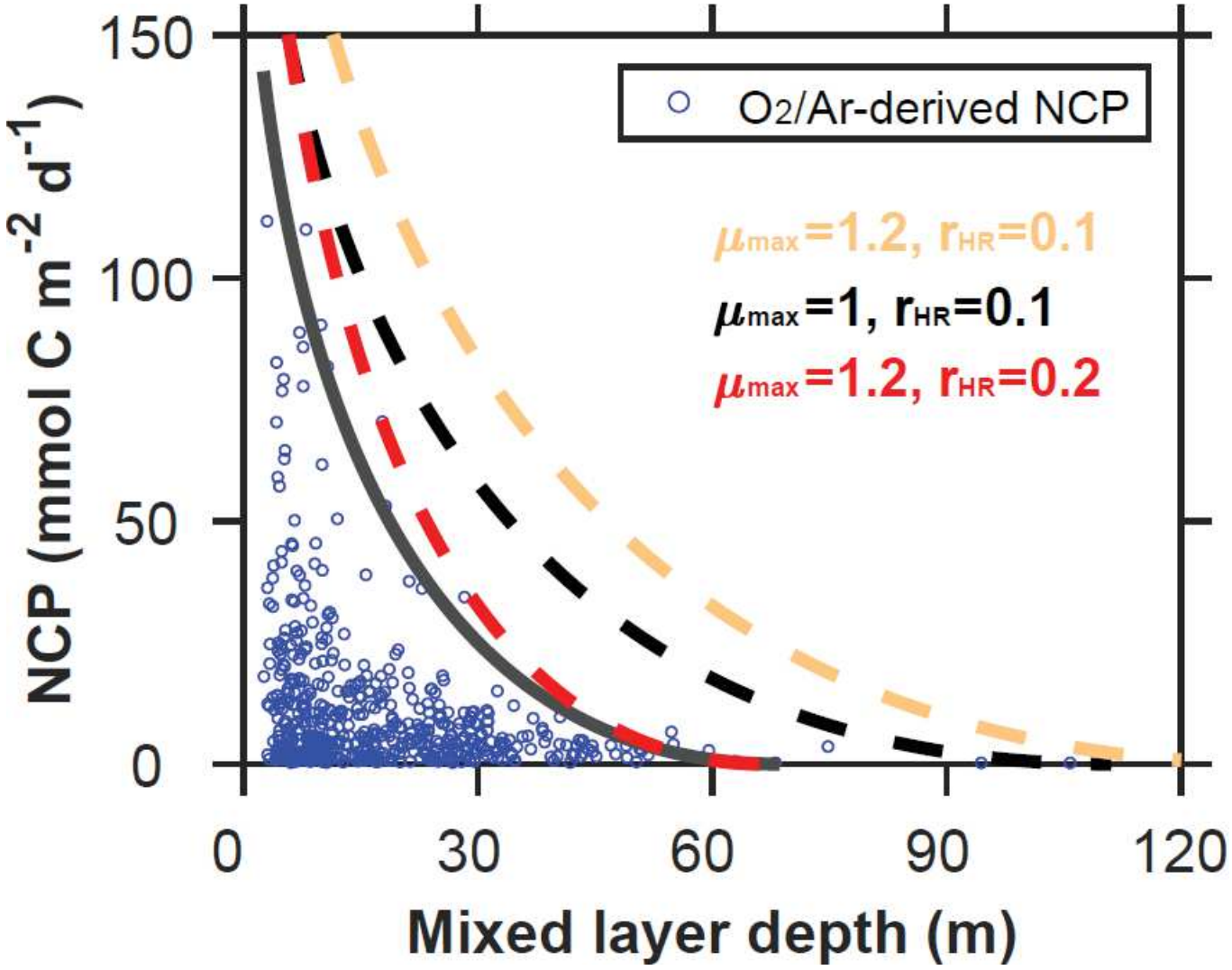

Figure S4. Modeled upper bound on carbon export production compared to field observations as a function of mixed layer depth (MLD). Observations are based on O_2/Ar-derived net community production (NCP). To account for the effect of photosynthetically active radiation (PAR) on export production, both MLD and carbon fluxes are normalized to $-log(1 - I_m(0))$ (see equations (19) and (21)). The thick gray line represents the upper bound fitted to the NCP data. Dash-lines represent the upper bounds calculated using parameters available in the literature (Table 2). A stoichiometric ratio of O_2/C=1.4 was used to convert NCP from O_2 to C units (Laws, 1991).

References

Arrigo, K. R., van Dijken, G. L., and Bushinsky, S.: Primary production in the Southern Ocean, 1997-2006, J. Geophys. Res., 113, doi:10.1029/2007JC004551, 2008.

Bender, M. L., Kinter, S., Cassar, N., and Wanninkhof, R.: Evaluating gas transfer velocity parameterizations using upper ocean radon distributions, J. Geophys. Res., 116, doi:10.1029/2009JC005805, 2011.

Cael, B. B. and Follows, M. J.: On the temperature dependence of oceanic export efficiency, Geophys. Res. Lett., 43, 5170-5175, doi:10.1002/2016GL068877, 2016.

Cassar, N., Nevison, C. D., and Manizza, M.: Correcting oceanic O_2/Ar-net community production estimates for vertical mixing using N_2O observations, Geophys. Res. Lett., 41, 8961-8970, doi:10.1002/2014GL062040, 2014.

Cassar, N., Bender, M. L., Barnett, B. A., Fan, S., Moxim, W. J., Levy, H., and Tilbrook, B.: The Southern Ocean biological response to aeolian iron deposition, Science, 317, 1067-1070, doi:10.1126/science.1144602, 2007.

Cassar, N., DiFiore, P. J., Barnett, B. A., Bender, M. L., Bowie, A. R., Tilbrook, B., Petrou, K., Westwood, K. J., Wright, S. W., and Lefevre, D.: The influence of iron and light on net community production in the Subantarctic and Polar Frontal Zones, Biogeosciences, 8, 227-237, doi:10.5194/bg-8-227-2011, 2011.

Craig, H. and Hayward, T.: Oxygen supersaturation in the ocean: Biological versus physical contributions, Science, 235, 199-202, doi:10.1126/science.235.4785.199, 1987.

de Boyer Montegut, C., Madec, G., Fischer, A. S., Lazar, A., and Iudicone, D.: Mixed layer depth over the global ocean: An examination of profile data and a profile-based climatology, Journal of Geophysical Research-Oceans, 109, doi:10.1029/2004JC002378, 2004.

Dong, S., J. Sprintall, Gille, S. T., and Talley, L.: Southern Ocean mixed-layer depth from Argo float profiles, Journal of Geophysical Research-Oceans, 113, doi:10.1029/2006JC004051, 2008.

Eveleth, R., Timmermans, M. L., and Cassar, N.: Physical and biological controls on oxygen saturation variability in the upper Arctic Ocean, Journal of Geophysical Research-Oceans, 119, 7420-7432, doi:10.1002/2014JC009816, 2014.

Eveleth, R., Cassar, N., Sherrell, R. M., Ducklow, H., Meredith, M., Venables, H., Lin, Y., and Li, Z.: Ice melt influence on summertime net community production along the Western Antarctic Peninsula, Deep Sea Research Part II., 139, 89-102, doi:10.1016/j.dsr2.2016.07.016, 2017.

Hamme, R. C., Cassar, N., Lance, V. P., Vaillancourt, R. D., Bender, M. L., Strutton, P. G., Moore, T. S., DeGrandpre, M. D., Sabine, C. L., Ho, D. T., and Hargreaves, B. R.: Dissolved O_2/Ar and other methods reveal rapid changes in productivity during a Lagrangian experiment in the Southern Ocean, Journal of Geophysical Research-Oceans, 117, doi:10.1029/2011JC007046, 2012.

Huang, K., Ducklow, H., Vernet, M., Cassar, N., and Bender, M. L.: Export production and its regulating factors in the West Antarctica Peninsula region of the Southern Ocean, Global Biogeochem Cy, 26, doi:10.1029/2010GB004028, 2012.

Jonsson, B. F., Doney, S. C., Dunne, J. P., and Bender, M. L.: Evaluation of the Southern Ocean O_2/Ar-based NCP estimates in a model framework, Journal of geophysical Research, 118, 385-399, doi:10.1002/jgrg.20032, 2013.

Juranek, L. W., Hamme, R. C., Kaiser, J., Wanninkhof, R., and Quay, P. D.: Evidence of O_2 consumption in underway seawater lines: Implications for air-sea O_2 and CO_2 fluxes, Geophys Res Lett, 37, doi:10.1029/2009GL040423, 2010.

Li, Z. and Cassar, N.: Satellite estimates of net community production based on O_2/Ar observations and comparison to other estimates, Global Biogeochem Cy, 30, 735-752, doi:10.1002/2015GB005314, 2016.

Martin, J. H., Knauer, G. A., Karl, D. M., and Broenkow, W. W.: VERTEX: Carbon Cycling in the Northeast Pacific, Deep Sea Research Part A., 34, 267-285, doi:10.1016/0198-0149(87)90086-0, 1987.

Martin, P., van der Loeff, M. R., Carssar, N., Vandromme, P., d'Ovidio, F., Stemmann, L., Rengarajan, R., Soares, M., González, H. E., Ebersbach, F., Lampitt, R. S., Sanders, R., Barnett, B. A., Smetacek, V., and Naqvi, S. W. A.: Iron fertilization enhanced net community production but not downward particle flux during the Southern Ocean iron fertilization experiment LOHAFEX, Global Biogeochem Cy, 27, 871-881, doi:10.1002/gbc.20077, 2013.

Mouw, C. B., Barnett, A., McKinley, G. A., Gloege, L., and Pilcher, D.: Global ocean particulate organic carbon flux merged with satellite parameters, Earth System Science Data, 8, 531-541, doi:10.5194/essd-8-531-2016, 2016.

Reuer, M. K., Barnett, B. A., Bender, M. L., Falkowski, P. G., and Hendricks, M. B.: New estimates of Southern Ocean biological production rates from O_2/Ar ratios and the triple isotope composition of O_2, Deep Sea Research Part I, 54, 951-974, doi:10.1016/j.dsr.2007.02.007, 2007.

Shadwick, E. H., Tilbrook, B., Cassar, N., Trull, T. W., and Rintoul, S. R.: Summertime physical and biological controls on O_2 and CO_2 in the Australian Sector of the Southern Ocean, J Marine Syst, 147, 21-28, doi:10.1016/j.jmarsys.2013.12.008, 2015.

Stanley, R. H. R., Kirkpatrick, J. B., Cassar, N., Barnett, B. A., and Bender, M. L.: Net community production and gross primary production rates in the western equatorial Pacific, Global Biogeochem Cy, 24, doi:10.1029/2009GB003651, 2010.

Tortell, P. D., Gueguen, C., Long, M. C., Payne, C. D., Lee, P., and DiTullio, G. R.: Spatial variability and temporal dynamics of surface water pCO_2, ΔO_2/Ar and dimethylsulfide in the Ross Sea, Antarctica, Deep Sea Research Part I, 58, 241-259, doi:10.1016/j.dsr.2010.12.006, 2011.

Wanninkhof, R.: Relationship between wind speed and gas exchange over the Ocean, Journal of Geophysical Research-Oceans, 97, 7373-7382, doi:10.1029/92JC00188, 1992.

Werdell, P. J. and Bailey, S. W.: An improved in-situ bio-optical data set for ocean color algorithm development and satellite data product validation, Remote Sensing of Environment, 98, 122-140, doi:10.1016/j.rse.2005.07.001, 2005.